UNIVERSITÀ DEGLI STUDI DI PADOVA

Dipartimento di Fisica e Astronomia "Galileo Galilei"

Master Degree in Physics

Final Dissertation

Higgs production in vector boson fusion at lepton colliders in SMEFT

Thesis supervisors

Prof. Ramona Gröber

Prof. Gudrun Heinrich

Thesis co-supervisors

Dr. Stefano Di Noi

Dr. Marius Höfer

Candidate

Silvia Pigozzi

Academic Year 2025/2026

Ai miei genitori e
a mio fratello Luca.

Abstract

In this thesis, we describe the first stages of the implementation with GoSam of single Higgs production at a future e^+e^- collider within the framework of Standard Model Effective Field Theory (SMEFT). Studying SMEFT effects at such high energies is crucial to disentangle different new physics footprints or, alternatively, to set robust bounds on them.
Our focus will be on Higgs production via vector boson fusion, which becomes increasingly relevant at center-of-mass energies above 300 GeV compared to the Higgstrahlung production channel which, instead, is dominant at low energies. One of the aspects of this thesis is to study the relevance of the interference at leading order between the two production mechanisms, to justify the separate treatments of the two.
Up to now, SMEFT effects in vector boson fusion have been investigated only at leading order. However, to fully exploit the discovery potential of a future collider, next-to-leading order electroweak corrections must be included. These corrections not only improve the precision of the predictions, but are also particularly relevant because they become sensitive to operators that do not contribute at leading order.
Finally, we discuss the progress that has been achieved in the implementation of the process, together with the validations steps that have been taken so far.

Contents

Chapter 1

Introduction

The Standard Model (SM) of particle physics is the quantum field theory that describes how the basic constituents of matter, the fermions, interact via weak, strong and electromagnetic forces. SM predictions have been experimentally confirmed at colliders with extraordinary precision, making it one of the greatest achievements of modern physics. Nevertheless, some experimental observations suggest that the model is not complete. Indeed, it does not explain the baryon asymmetry of the universe and the presence of dark matter and dark energy. There are also some limits within its theoretical formulation, for example the exclusion of gravity among its particle interactions, the hierarchy problem for the Higgs mass or the impossibility to define a non-vanishing mass for neutrinos.

In order to address these problems, a large number of theories Beyond the Standard Model (BSM) have been proposed, but none of these models has achieved experimental confirmation so far. An alternative approach is to parametrize deviations from the SM using an effective field theory. In this scenario, the SM is the low-energy description of a more fundamental theory, whose new heavy degrees of freedom are integrated out and the resulting theory contains only effective interactions among SM fields. The effective Lagrangian consists of a series of local interaction operators of increasing dimension and relative effective couplings, known as Wilson Coefficients (WCs). Within this thesis, we employ the Standard Model Effective Field Theory (SMEFT).

In order to compare the theoretical predictions with the measurements from particle collider experiments, quantum corrections must be included. Predictions for New Physics (NP) at high energies can be made more robust if quantum corrections are included not only in the SM, but also in the SMEFT. Next-to-leading order (NLO) corrections in dimension-six SMEFT are almost fully automatized for Quantum Chromo-Dynamics (QCD) [1]. This is not the case for electroweak (EW) corrections, which must be calculated for each specific process.

This thesis focuses on the study of the Higgs production mechanisms at future electron-positron colliders, which in the following we assume to be the FCC-ee [2], within the SMEFT. At low energies, the predominant channel is Higgsstrahlung (HS), $e^+e^- \to Zh$, motivating a dedicated experimental run at $\sqrt{s} = 240$ GeV where a maximum is reached. This channel has already been studied in detail and the quantum corrections at NLO in the SMEFT can be found in [3]. Instead, we focus on the collider run at $\sqrt{s} = 350$ or 365 GeV, where the Vector Boson Fusion (VBF) mechanism, $e^+e^- \to \nu\bar{\nu}h$, becomes more relevant for a final state with a Higgs and two electron neutrinos. We show the predominance of VBF with respect to HS at these higher energies, studying as well the interplay between the two via interference effects, and we set the stage for the

renormalization of its SMEFT matrix element. We compute the counterterms needed to implement the UV renormalization within the SM and check that they cancel the UV pole of the 1-loop amplitude. In the literature, the NLO corrections in the SM and the NLO cross sections can be found in [4]-[5]. However, in this thesis, we present the UV pole of the analytic gauge-independent expressions for the counterterms and the UV pole of the NLO amplitude.
Studying this process at $\sqrt{s}$ >350GeV within the SMEFT is advantageous because NLO corrections become sensitive to NP operators not contributing at TL and, therefore, NP effects could be uncovered. In [6], the numerical LO and NLO cross sections are presented for the SM and the Two-Higgs Doublet Model (2HDM). However, a full implementation within the SMEFT has not yet been presented. We perform our computation with GoSam [7] , a program for automated calculation of one-loop amplitudes. In what follows, we describe the status of this program, describing in detail the computational and conceptual aspects that have been studied.
The present thesis is organized as follows. Chapter 2 provides an overview of the SM: the gauge group and the particle content are presented, together with a detailed description of the different sectors of the SM Lagrangian. Moreover, we briefly describe its limitations. In Chapter 3 the two main approaches (Top-Down and Bottom-Up) to the usage of EFTs are presented. We also introduce and discuss the SMEFT in order to establish the conventions used throughout the thesis. Chapter 4 investigates the interplay between VBF and HS at $\sqrt{s} = 350$ GeV by studying how large the interference between the two production mechanisms could be in the SMEFT. Moreover, truncation effects on the total cross section are studied, in order to keep under control the convergence of the EFT expansion. Chapter 5 provides the theoretical framework for the implementation of the EW NLO corrections to VBF: the basis of dimension-six SMEFT operators contributing at NLO to the VBF is presented and the ultraviolet (UV) renormalization in the Fleischer-Jegerlehner (FJ) tadpole scheme [8] is discussed. Furthermore, we describe the treatment of the infrared (IR) divergences.
Chapter 6 provides the analytic result of the VBF renormalization within the SM in the FJ scheme and its matching with the numerical result from GoSam. Finally, we present our conclusions and discuss the outlook for further studies in Chapter 7.

Chapter 2

The Standard Model of Particle Physics

The Standard Model (SM) of particle physics provides a successful description of the fundamental constituents of matter and their strong and electroweak interactions. The SM does not describe gravity which, being much weaker than the other interactions, becomes only relevant at high energies, close to the Planck scale.
The SM provides a consistent theoretical framework to compute observables relevant at particle collider experiments, being its last founding prediction the discovery of the Higgs boson in 2012.
Despite a large number of precision experiments have proven the SM to be a very good description of particle physics, there are still open questions that need to be addressed in the future. Many phenomena, such as the presence of dark matter in the universe or the hierarchy problem of the SM Higgs boson, suggest, indeed, that the SM must be extended.
In this first chapter, a brief description of the four categories of particles of the SM is provided, together with the mathematical framework defining their interactions. As any other model of particle physics, the SM has to be constructed specifying the gauge group of the theory, together with the possibility of a Spontaneous Symmetry Breaking (SSB) into a smaller group, and the particle content.

2.1 The gauge group

The gauge group of the theory is:

$$G_{\text{SM}} = SU(3)_C \otimes SU(2)_L \otimes U(1)_Y, \tag{2.1}$$

where

- $SU(3)_C$ describes strong interactions. It has 8 generators, namely $\lambda^a/2$, where λ^a are the Gell-Mann matrices; as a consequence, there are 8 gluon fields G^a_μ, $a = 1, ..., 8$ that transform in the adjoint representation of the gauge group.

- $SU(2)_L \otimes U(1)_Y$ describes electro-weak interactions.
  - $SU(2)_L$ has 3 generators, $\sigma^i/2$, where σ^i are the Pauli matrices satisfying the commutation relation $[\sigma_i, \sigma_j] = 2i\epsilon_{ijk}\sigma_k$; thus, there are 3 vector bosons W^i_μ, $i = 1, 2, 3$.

– $U(1)_Y$ has 1 generator, $Y/2$, where Y is the hypercharge, and therefore it is associated to 1 vector boson B_μ.

The introduced gauge bosons G^a_μ, W^i_μ, B_μ are defined in the following subsection.

2.2 The particle content

In the SM, all matter in the universe is made up of elementary particles that can be grouped into four categories, according to their quantum numbers and the ways they interact with other particles: gauge bosons, quarks, leptons and the Higgs scalar.

Gauge bosons

The gauge fields are massless vector bosons with two degrees of freedom. Their transformations under G_{SM} are:

$$G^a_\mu \sim (\mathbf{8}, \mathbf{1}, 0), \qquad W^i_\mu \sim (\mathbf{1}, \mathbf{3}, 0), \qquad B_\mu \sim (\mathbf{1}, \mathbf{1}, 0). \tag{2.2}$$

The first two numbers in bold denote the $SU(3)_C$ and $SU(2)_L$ representation (in this order), while the third number denotes the field hypercharge. The gluon fields G^a_μ transform indeed under the adjoint representation of $SU(3)_C$ and W^i_μ under the adjoint representation of $SU(2)_L$.

Quarks

The quarks are fermions with fractional electric charges and are subject to both strong and electroweak interactions. As all fermions, they are classified into three generations, which differ only by the fermion masses. In the following, the subscripts L and R refer to the left and right two-component Weyl spinors in which fermions can be decomposed by acting on the dimension-four Dirac spinor Ψ with the left and right projectors

$$\Psi_L = \mathcal{P}_L \Psi = \frac{\mathbb{1} - \gamma_5}{2}\Psi \quad \text{and} \quad \Psi_R = \mathcal{P}_R \Psi = \frac{\mathbb{1} + \gamma_5}{2}\Psi. \tag{2.3}$$

The Lorentz group is instead locally isomorphic to two independent copies of the $SU(2)$ algebra, $SU(2)^{\text{spin}}_L \otimes SU(2)^{\text{spin}}_R$, labeled by two spins (j_L, j_R). If, for example, $j_L = 1/2$ and $j_R = 0$, fermions transform non-trivially only under $SU(2)^{\text{spin}}_L$. This is the case for left-handed fermions that belong to the $(1/2, 0)$ representation of the Lorentz group and act as doublets under the weak isospin $SU(2)_L$ group of G_{SM}; right-handed fermions belong instead to the $(0, 1/2)$ representation of the Lorentz group and are $SU(2)_L$ singlets:

$${q_L}^i = \left\{ \begin{pmatrix} u_L \\ d_L \end{pmatrix}, \begin{pmatrix} c_L \\ s_L \end{pmatrix}, \begin{pmatrix} t_L \\ b_L \end{pmatrix} \right\}, \qquad u^i_R = \{u_R, c_R, t_R\}, \qquad d^i_R = \{d_R, s_R, b_R\}. \tag{2.4}$$

They transform under G_{SM} as:

$$q^i_L \sim (\mathbf{3}, \mathbf{2}, 1/6), \qquad u^i_R \sim (\mathbf{3}, \mathbf{1}, 2/3), \qquad d^i_R \sim (\mathbf{3}, \mathbf{1}, -1/3). \tag{2.5}$$

As shown in eq. (2.5), all quarks transform under the fundamental representation of $SU(3)_C$, as they interact via strong interaction. Strong interactions feature the so-called color confinement: at energies $\lesssim 1$ GeV the quarks are only found in bound states, called hadrons. They are held together by gluons, the mediators of the strong force.

Leptons

Leptons are fermions with electric charge -1 or 0. They are subject to electroweak interactions, but they do not couple to gluons. As for the quarks, they are divided into three generations, with left and right-handed fermions belonging to the $(1/2, 0)$ and $(0, 1/2)$ representation of the Lorentz group, respectively:

$$
{l_L}^i = \left\{ \begin{pmatrix} \nu_{eL} \\ e_L \end{pmatrix}, \begin{pmatrix} \nu_{\mu L} \\ \mu_L \end{pmatrix}, \begin{pmatrix} \nu_{\tau L} \\ \tau_L \end{pmatrix} \right\}, \qquad e_R^i = \{e_R, \mu_R, \tau_R\}. \tag{2.6}
$$

In this thesis, neutrinos are assumed to be massless; hence, there is no need to introduce right-handed neutrinos, as detailed in section 2.3.4. Leptons transform under G_{SM} as:

$$
l_L^i \sim (\mathbf{1}, \mathbf{2}, -1/2), \qquad e_R^i \sim (\mathbf{1}, \mathbf{1}, -1). \tag{2.7}
$$

Higgs scalar

The only scalar of the Standard Model is the Higgs scalar, a complex $SU(2)$ doublet:

$$
\varphi = \begin{pmatrix} \varphi_+ \\ \varphi_0 \end{pmatrix} = \begin{pmatrix} \phi_1 + i\phi_2 \\ \phi_3 + i\phi_4 \end{pmatrix}, \tag{2.8}
$$

where $\phi_{1,2,3,4}$ are real scalar fields. Under G_{SM}, it transforms as:

$$
\varphi \sim (\mathbf{1}, \mathbf{2}, 1/2). \tag{2.9}
$$

Under the assumption that its potential produces a stable and non-vanishing vacuum, the SSB of the SM gauge group G_{SM} into the smaller group

$$
G = SU(3)_C \otimes U(1)_{em} \tag{2.10}
$$

can occur, providing mass terms for all the massive particles of the SM, as detailed in section 2.3.2.

2.3 The Standard Model Lagrangian

The most general SM Lagrangian, invariant under G_{SM}, can be schematically written as:

$$
\begin{aligned}
\mathcal{L}_{\text{SM}} &= -\frac{1}{4} F^{\mu\nu} F_{\mu\nu} + i\bar{\Psi}\gamma^\mu D_\mu \Psi + (D_\mu \varphi)^\dagger (D^\mu \varphi) - V(\varphi^\dagger \varphi) + (\bar{\Psi} Y \varphi \Psi + \text{h.c.}) \\
&= \mathcal{L}_{kin}^{g.b.} + \mathcal{L}_{kin}^{f} + \mathcal{L}_{kin}^{\varphi} + \mathcal{L}_{pot}^{\varphi} + \mathcal{L}_Y .
\end{aligned} \tag{2.11}
$$

In the following, the different sectors of $\mathcal{L}_{\text{SM}}$ are analyzed separately.

2.3.1 The bosonic sector

The gauge boson kinetic Lagrangian is

$$\mathcal{L}^{g.b.}_{kin} = -\frac{1}{4}F^{\mu\nu}F_{\mu\nu} \supset -\frac{1}{4}W^{\mu\nu,i}W^{i}_{\mu\nu} - \frac{1}{4}B^{\mu\nu}B_{\mu\nu}, \qquad i = 1,2,3 \tag{2.12}$$

where the field strength tensors are defined as

$$\begin{aligned} W^{i}_{\mu\nu} &= \partial_\mu W^i_\nu - \partial_\nu W^i_\mu + g\epsilon^{ijk}W^j_\mu W^k_\nu, \\ B_{\mu\nu} &= \partial_\mu B_\nu - \partial_\nu B_\mu. \end{aligned} \tag{2.13}$$

The gluon fields are not included since they are not relevant for the purposes of this thesis.
From the first term in eq. (2.12), we expect triple and quartic self interactions among gauge bosons, as a consequence of the non-abelian EW structure of the SM.
The gauge transformations for the electroweak (EW) sector in the fundamental representation are

$$U(\theta(\vec{x})) = e^{-i\vec{\theta}(x)\cdot\frac{\vec{\sigma}}{2}} \in SU(2)_L, \qquad U(\beta(x)) = e^{-i\beta(x)Y} \in U(1)_Y \tag{2.14}$$

and they transform the gauge fields in the following way:

$$\begin{aligned} \vec{\sigma}\cdot\vec{W}'_\mu &= U(\theta)(\vec{\sigma}\cdot\vec{W}_\mu)U(\theta)^{-1} + \frac{i}{g}U(\theta)\partial_\mu U(\theta)^{-1}, \\ B'_\mu &= B_\mu + \frac{1}{g'}\partial_\mu\beta(x), \end{aligned} \tag{2.15}$$

where g and g' are the coupling constants of, respectively, $SU(2)_L$ and $U(1)_Y$.

2.3.2 The Higgs Sector

The Higgs kinetic term is written in terms of the covariant derivative

$$D_\mu\varphi = \Big(\partial_\mu - ig\frac{\vec{\sigma}}{2}\cdot\vec{W}_\mu - ig'Y_\varphi B_\mu\Big)\varphi, \tag{2.16}$$

where $\sigma^i/2$ are the three $SU(2)$ generators and $Y_\varphi = 1/2$ is the Higgs hypercharge.
The potential of the Higgs doublet can instead be written as:

$$V(|\varphi|^2) = \frac{\lambda}{4}\left(|\varphi|^2 - \frac{v^2}{2}\right)^2, \qquad \text{where} \quad |\varphi|^2 = \varphi^\dagger\varphi. \tag{2.17}$$

λ must be positive to have a potential bounded from below and the coefficient of $|\varphi|^2$ is negative to realize a SSB of the theory, as detailed in the following.

Electroweak Spontaneous Symmetry Breaking

The Higgs potential has a relative minimum at $|\varphi| = v/\sqrt{2}$ and therefore, using the polar parametrization, yields

$$\varphi(x) = \begin{pmatrix} 0 \\ \frac{\rho(x)}{\sqrt{2}} \end{pmatrix} e^{i\frac{\zeta^i(x)\tau^i}{v}}, \tag{2.18}$$

where four scalar fields $\rho(x)$ and $\zeta^i(x)$ (i=1,2,3) have been introduced.
One can write $\rho(x) = v + h(x)$, where the Higgs scalar field $h(x)$ represents the fluctuations of $\rho(x)$ around the minimum of the potential. ζ^i are instead the three Goldstone bosons and they represent the fluctuations of φ along the flat directions of the potential. They are associated to the broken generators of $SU(2)_L \otimes U(1)_Y$, which are τ_1, τ_2 and $\tau_3 - Y/2$. The EW symmetry of the theory is indeed broken as

$$SU(2)_L \otimes U(1)_Y \Longrightarrow U(1)_{\text{em}} \tag{2.19}$$

and the unbroken generator of $U(1)_{\text{em}}$ is the electric charge $Q = \tau_3 + Y/2$. We stress that the vacuum of the theory is invariant under $U(1)_{em}$ transformations.

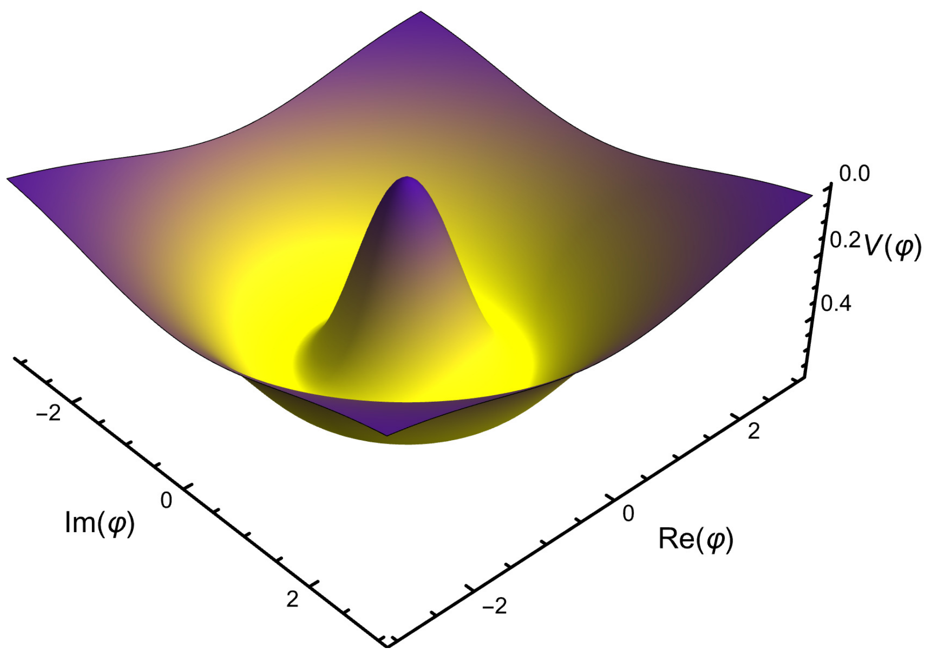

Figure 2.1: Visual representation of the Higgs potential. The minima of the potential can be found going towards the yellow region.

There is a dependence on $\rho(x)$ in $V(|\varphi|^2)$ and, in particular, substituting $\rho(x) = v + h(x)$ inside the potential, one can find the mass for the scalar Higgs field:

$$V(h(x)) = \frac{\lambda}{16}((v+h(x))^2 - v^2)^2 = \frac{1}{2}\underbrace{\frac{1}{2}\lambda v^2}_{M_h^2} h(x)^2 + \frac{\lambda}{4} v h(x)^3 + \frac{\lambda}{16} h(x)^4. \tag{2.20}$$

If we exploit the unitary gauge (UG), where $\zeta^i(x) = 0$, then the masses for the EW massive bosons defined as

$$W^\pm_\mu = \frac{W^1_\mu \mp iW^2_\mu}{\sqrt{2}}, \tag{2.21}$$

$$Z_\mu = c_W W^3_\mu - s_W B_\mu \tag{2.22}$$

and for the photon field

$$A_\mu = c_W B_\mu + s_W W^3_\mu \tag{2.23}$$

are manifest from the kinetic term of the Higgs doublet $\mathcal{L}^\varphi_{kin}$.
s_W and c_W are, respectively, the sine and cosine of the so-called Weinberg angle, whose tangent is defined as the ratio of the $U(1)_Y$ and $SU(2)_L$ coupling constants:

$$t_W = \frac{g'}{g}, \tag{2.24}$$

and has an experimental value of

$$s^2_W \simeq 0.22.$$

Before SSB, the gauge bosons W^i_μ and B_μ are massless, with two polarization states. When the gauge symmetry is spontaneously broken, the degree of freedom of the Goldstone bosons is absorbed by the gauge fields in $\mathcal{L}^\varphi_{kin}$, providing the longitudinal polarization of massive spin-1 particles.
The mass spectrum before and after SSB is:

before SSB			after SSB		
particle	squared mass	d.o.f.	particle	squared mass	d.o.f.
φ	$\frac{\lambda v^2}{2}$	4	h	$\frac{\lambda v^2}{2}$	1
W^i_μ	0	3×2	$W^\pm_\mu$	$\frac{g^2 v^2}{4}$	2×3
B_μ	0	2	Z_μ	$\frac{g^2+g'^2}{4}$	3
			A_μ	0	2

Table 2.1: Boson mass spectrum before and after EW SSB.

After SSB, the Goldstones do not appear anymore in the UG in the physical spectrum since they have already provided the missing degree of freedom for the longitudinal polarization of the massive gauge bosons.
In the UG, the expectation value for the complex field φ is chosen such that its phase is zero. In this special case, all the Goldstone fields disappear from the Lagrangian.
The complete Higgs sector of the SM Lagrangian in the UG is:

$$\begin{aligned}(\mathcal{L}^\varphi_{kin} + \mathcal{L}^\varphi_{pot})|_{u.g.} = \frac{1}{2}(\partial_\mu h)(\partial^\mu h) - \frac{1}{2}M^2_h h^2 + \frac{(v+h)^2}{4} g^2 W^+_\mu W^{-\mu} + \\ \frac{(v+h)^2}{2}\frac{(g^2+g'^2)}{4} Z_\mu Z^\mu - \lambda v h^3 - \frac{\lambda}{4} h^4.\end{aligned} \tag{2.25}$$

Conversely, in a different gauge, the Goldstones can still be explicitly present in the Lagrangian; however they are unphysical and, indeed, they do not appear as external states in physical processes.

R_ξ gauges

In R_ξ gauges, the Goldstone bosons do not appear as explicit degrees of freedom in the spectrum. In the Lagrangian, after SSB, the gauge bosons mix with the Goldstone fields. As a consequence, the quadratic part of the Lagrangian is not diagonal in the gauge and Goldstone fields, and the propagators are therefore not immediately well defined. These gauge-Goldstone bosons mixing terms are not present in the unitary gauge, where the quadratic operators produce the following propagators for massive vector bosons:

$$\Pi^{u.g.}_{X,\mu\nu} = \frac{i}{p^2 - M_X^2}\bigg(- g_{\mu\nu} + \frac{p_\mu p_\nu}{M_X^2}\bigg), \qquad X = Z, W^\pm. \tag{2.26}$$

Nevertheless, it is not convenient to use the unitary gauge in practical computations because the term proportional to $p_\mu p_\nu$ in eq. (2.26) leads to a worse ultraviolet behaviour in intermediate loop integrals.
In R_ξ gauges, the Lorentz-invariant gauge-fixing terms

$$-\frac{(\partial_\mu Z^\mu - \xi_Z m_Z \chi)^2}{2\xi_Z} \qquad \text{and} \qquad -\frac{(\partial^\mu W^+_\mu - i\xi_W m_W \varphi^+)(\partial^\nu W^-_\nu + i\xi_W m_W \varphi^-)}{\xi_W} \tag{2.27}$$

are added to the Lagrangian in order to eliminate the gauge-Goldstone bosons mixing terms. This procedure yields diagonal quadratic terms for both the Goldstone and the gauge boson fields, leading to the following propagators:

$$\Pi^{R_\xi}_{X,\mu\nu} = \frac{-ig_{\mu\nu}}{p^2 - M_X^2} + \frac{ip_\mu p_\nu}{M_X^2}\bigg(\frac{1}{p^2 - M_X^2} - \frac{1}{p^2 - \xi_X M_X^2}\bigg), \tag{2.28}$$

$$\Pi_\chi = \frac{i}{p^2 - \xi_Z M_Z^2}, \qquad \Pi_{\varphi^\pm} = \frac{i}{p^2 - \xi_W M_W^2} \tag{2.29}$$

where $X = Z, W^\pm$, χ is the neutral and $\varphi^\pm$ the charged Goldstone bosons.
In R_ξ gauges the Goldstone bosons have an unphysical mass-squared $\xi_X M_X^2$, where ξ_X are arbitrary real gauge-fixing parameters. The limit $\xi_X \to \infty$ reproduces the unitary gauge, as the Goldstones do not propagate anymore. Since physical quantities are gauge independent, quantities such as scattering amplitudes and cross sections must be independent on ξ_X.
A gauge fixing term is needed also for the photon field. The term of $\mathcal{L}^{g.b.}_{kin}$ quadratic in the photon field A_μ contains the operator

$$\partial_\mu \partial_\nu - \Box g_{\mu\nu} \tag{2.30}$$

which is not invertible. This problem originates from the gauge invariance of electromagnetism. $\mathcal{L}_{\text{SM}}$ is invariant under the transformation in eq. (2.31)

$$A_\mu \to A_\mu + \partial_\mu \Lambda(X), \tag{2.31}$$

where $\Lambda(X)$ is a scalar function. If the operator in eq. (2.30) is applied to $A_\mu = \partial_\mu \Lambda(X)$, it gives zero:

$$(\partial_\mu \partial_\nu - \Box g_{\mu\nu})\partial^\mu \Lambda = (\Box p_\nu - \Box p_\nu)\Lambda = 0 \tag{2.32}$$

The quadratic operator becomes invertible only after fixing the gauge. This is done by adding the gauge fixing term

$$-\frac{(\partial^\mu A_\mu)(\partial^\nu A_\nu)}{2\xi_A} \tag{2.33}$$

to the Lagrangian, depending on an arbitrary real parameter ξ_A. This produces the following photon propagator:

$$\Pi^{R_\xi}_{A,\mu\nu} = \frac{-ig_{\mu\nu}}{p^2} + (1-\xi_A)\frac{ip_\mu p_\nu}{p^4}. \tag{2.34}$$

The Feynman gauge $\xi_A = \xi_Z = \xi_W = 1$ eliminates the longitudinal momentum-dependent terms in the numerator of the vector bosons propagators.
In this thesis, all the computations are performed in the Feynman gauge in order to simplify intermediate expressions and improve the ultraviolet behavior of propagators in loop computations in `GoSam`.

2.3.3 The Yukawa sector

The Yukawa sector of the SM Lagrangian, before SSB, reads:

$$\mathcal{L}_Y = -(\bar{q}_L)_i (Y_u)_{ij} \tilde{\varphi} (\bar{u}_R)_j - (\bar{q}_L)_i (Y_d)_{ij} \varphi (d_R)_j - (\bar{l}_L)_i (Y_e)_{ij} \tilde{\varphi} (e_R)_j + h.c., \tag{2.35}$$

where the conjugate Higgs doublet has been introduced, defined as:

$$\tilde{\varphi} = i\sigma_2 \varphi^* = i \begin{pmatrix} 0 & -i \\ i & 0 \end{pmatrix} \begin{pmatrix} \phi_1 - i\phi_2 \\ \phi_3 - i\phi_4 \end{pmatrix} = \begin{pmatrix} \phi_3 - i\phi_4 \\ -\phi_1 + i\phi_2 \end{pmatrix}. \tag{2.36}$$

It is possible to diagonalize the Yukawa matrices by applying the following field rotations:

$$\begin{cases} u'_L = L_u u_L \\ d'_L = L_d d_L \\ e'_L = L_e e_L \end{cases}, \qquad \begin{cases} u'_R = R_u u_R \\ d'_R = R_d d_R \\ e'_R = R_e e_R \end{cases}, \tag{2.37}$$

where L and R are unitary 3×3 matrices in flavour space and the primed fields denote the new mass eigenstates.
The Yukawa sector of the SM Lagrangian after SSB, written in the unitary gauge and in the new mass basis, is:

$$\mathcal{L}_Y|_{u.g.} = -\frac{v+h}{\sqrt{2}} \left\{ (\bar{u}'_L)_i \underbrace{(L_u Y_u R_u^\dagger)_{ij}}_{(\hat{y}_u)_{ij}} (u'_R)_j + (\bar{d}'_L)_i \underbrace{(L_d Y_d R_d^\dagger)_{ij}}_{(\hat{y}_d)_{ij}} (d'_R)_j + (\bar{e}'_L)_i \underbrace{(L_e Y_e R_e^\dagger)_{ij}}_{(\hat{y}_e)_{ij}} (e'_R)_j \right\}.$$

These $\hat{y}_f$ ($f = u, d, e$) are diagonal matrices in flavour space and their eigenstates are real and proportional to the fermion masses:

$$(m_f)_{ii} = \frac{v}{\sqrt{2}} (\hat{y}_f)_{ii}. \tag{2.38}$$

2.3.4 The fermionic kinetic sector

The fermionic sector of the SM Lagrangian in the unitary gauge reads:

$$\begin{aligned}
\mathcal{L}_f|_{u.g.} = & \sum_f \bar{f}^i_L i\partial\!\!\!/ f^i_L + \sum_f \bar{f}^i_R i\partial\!\!\!/ f^i_R && \text{Kinetic terms} \\
& - \frac{g}{\sqrt{2}}\left(W^+_\mu \underbrace{(\bar{u}^i_L \gamma^\mu d^i_L + \bar{\nu}^i_L \gamma_\mu e^i_L)}_{J^{-\mu}} + W^-_\mu \underbrace{J^{+\mu}}_{(J^-_\mu)^\dagger} \right) && \text{Weak charged interaction} \\
& - \frac{g}{c_W} Z_\mu \sum_f \left(\bar{f}^i_L g^f_L \gamma^\mu f^i_L + \bar{f}^i_R g^f_R \gamma^\mu f^i_R \right) && \text{Weak neutral interaction} \\
& - eA_\mu \sum_f \left(\bar{f}^i_L \gamma^\mu f^i_L + \bar{f}^i_R \gamma^\mu f^i_R \right) Q_f && \text{Electromagnetic interaction}
\end{aligned}$$

where $f = e, u, d$ and $i = 1, 2, 3$ is the flavour index. The change of basis in eq. (2.37) affects only the weak charged interactions. Due to the unitarity of the L and R matrices, the kinetic sector is unaffected by the field rotations. The same happens to weak neutral and electromagnetic interactions. This stems from the commutativity of γ^μ and L/R matrices, since γ^μ acts in the spinor space while L and R act in the flavour space.
After applying the field rotations in eq. (2.37), the weak charged current yields:

$$\mathcal{L}_{CC} = -\frac{g}{\sqrt{2}}\left((\bar{u}'_L)_i \underbrace{(L_u L^\dagger_d)_{ij}}_{(V_{\text{CKM}})_{ij}} W\!\!\!\!/^+ (d'_L)_j + (\bar{v}'_L)_i \underbrace{(L_\nu L^\dagger_e)_{ij}}_{(U_{\text{PMNS}})_{ij}} W\!\!\!\!/^+ (e'_L)_j + h.c. \right), \tag{2.39}$$

where V_{CKM} and U_{PMNS} are flavour mixing unitary matrices. If right-handed neutrinos were introduced, the Yukawa sector would have had a new term with a yukawa coupling for neutrinos:

$$\mathcal{L}_Y \supset -(\bar{l}_L)_i (Y_\nu)_{ij} \varphi (\nu_R)_j + \text{h.c.}. \tag{2.40}$$

In the limit of massless neutrinos, that is $\hat{y_\nu} = 0$, it would be possible to choose whichever unitary matrix L_ν in order to write the Lagrangian in the neutrinos mass basis

$$\nu'_L = L_\nu \nu_L. \tag{2.41}$$

As a consequence, under the assumption that neutrinos are massless, one can choose $L_\nu = L_e$ and, therefore, U_{PMNS} (Pontecorvo-Maki-Sakata-Nakagawa) to be the identity matrix.
The quark flavour-mixing effects are instead given by the V_{CKM} (Cabibbo-Kobayashi-Maskawa) matrix:

$$V_{\text{CKM}} = L_u L^\dagger_d = \begin{pmatrix} V_{ud} & V_{us} & V_{ub} \\ V_{cd} & V_{cs} & V_{cb} \\ V_{td} & V_{ts} & V_{tb} \end{pmatrix}. \tag{2.42}$$

The V_{CKM} matrix is complex and unitary by construction and thus, it has nine real degrees of freedom, as one can realize by imposing $V^\dagger_{\text{CKM}} V_{\text{CKM}} = \mathbb{1}$. Only four of them are physical: 3 angles which describe the mixing between the three families of quarks and 1 phase that can not be eliminated. From precision flavour measurements, it turns out that the CKM matrix is nearly diagonal: the largest elements are on the diagonal, so flavour-changing transitions are suppressed. If one imposes exact flavour conservation in weak interactions, then also the CKM matrix reduces to the identity. This will be the case for the present thesis.

Chapter 3

Effective Field Theories

The energy scales involved in particle phenomenology span tens of orders of magnitudes, from atomic physics to cosmic rays. It is often not necessary to know in detail the laws at all energies to describe some processes at a given scale. If this is the case, then one can use an Effective Field Theory (EFT) with a limited range of applicability in the energy domain, which is usually simpler than the full theory. One example is classical mechanics, which is an effective theory of special relativity at small velocities $v \ll c$, written as an expansion in powers of the small parameter v^2/c^2 to the desired accuracy.
Three properties need to be specified in order to describe an EFT:

- The Lorentz and gauge symmetries of the model, which determine the allowed interactions among fields;
- The set of fields and their transformation properties under the symmetry of the model;
- The power counting, which is a set of rules allowing to organize the Lagrangian as a series expansion in terms of a small parameter E/Λ. Λ is called cut-off and is the scale at which the EFT ceases to be valid and E stands for the typical energy scale of the process. Clearly, it must hold $E \ll \Lambda$.

An EFT can be constructed following a Top-Down (TD) or a Bottom-Up (BU) approach.

Top-Down approach

In the TD approach, the EFT is used when its UV completion is known. It is useful to make precise predictions by integrating out heavy particles that are not dynamically relevant at low energies. With the TD approach one obtains an effective theory that accurately describes the physical system at low-energy scales and, at the same time, encodes the effects of the underlying high-energy theory within the Wilson Coefficients (WCs).
In order to derive the EFT Lagrangian from the full theory, the matching between the latter and the low-energy theory must be performed. In this way we ensure that both theories yield the same amplitudes at low energies, provided that the matrix element of the full theory is expanded in inverse power of m_h. Hence, the effect of the heavy particle that has been integrated out is incorporated in the low-energy WCs.

In the following, a more detailed description of the previous strategy is given.
The full theory Lagrangian depends on heavy fields, symbolically denoted by φ_h, with mass m_h, light fields φ_l with mass $m_l \ll m_h$ and generic coupling constants denoted by g.
The first step consists of constructing an effective Lagrangian, by integrating the heavy fields out:

$$\mathcal{L}_{\text{UV}}(\varphi_h, \varphi_l, g) \quad \Longrightarrow \quad \mathcal{L}_{\text{EFT}}(\varphi_l, c) \tag{3.1}$$

The EFT Lagrangian depends only on the light fields and on the new coupling constants denoted by c. The latter are the WCs.
We discuss now the example of a light Dirac fermion Ψ interacting with a heavy real scalar field Φ. The UV Lagrangian is:

$$\mathcal{L}_{\text{UV}}(\Phi, \Psi, \bar{\Psi}) = \bar{\Psi}(i\partial\!\!\!/ - m_l)\Psi + \frac{1}{2}\partial_\mu\Phi\partial^\mu\Phi - \frac{1}{2}m_h^2\Phi^2 - g\Phi\bar{\Psi}\Psi. \tag{3.2}$$

It is possible to obtain the effective Lagrangian by expressing the heavy field Φ in terms of the light ones from its equation of motion, in the limit $k^2 \ll m_h^2$, as in eq. (3.3)

$$\begin{aligned} &\partial_\mu\left(\frac{\partial\mathcal{L}}{\partial_\mu\Phi}\right) - \frac{\partial\mathcal{L}}{\partial\Phi} = 0 \\ &(\Box + m_h^2)\Phi = -g\bar{\Psi}\Psi \quad \Longrightarrow \Phi = -\frac{g}{m_h^2}\bar{\Psi}\Psi \end{aligned} \tag{3.3}$$

and by substituting this expression of Φ into the UV Lagrangian in eq. (3.2).
The EFT Lagrangian is:

$$\mathcal{L}_{\text{EFT}}(\Psi, \bar{\Psi}) = \bar{\Psi}(i\partial\!\!\!/ - m)\Psi + \frac{g^2}{2m_h^2}\bar{\Psi}\Psi\bar{\Psi}\Psi. \tag{3.4}$$

Diagrammatically, this means that, in the low energy limit in which the momentum of the scalar field k is much lower than its mass m_h, the interaction mediated by Φ for the $\Psi\bar{\Psi} \to \Psi\bar{\Psi}$ scattering is replaced with a 4-fermion interaction, as shown in Figure 3.1.

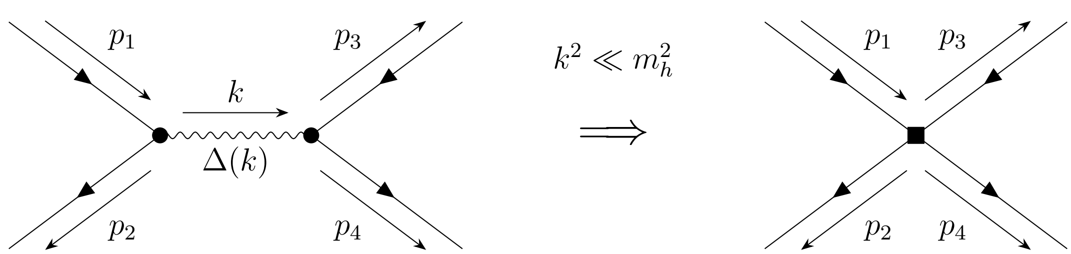

Figure 3.1: Diagrams in the full theory (left) and the EFT (right). The effective operator is represented with a black square dot.

In eq. (3.4), where the heavy field Φ has been integrated out, only its mass m_h appears in the coefficient of the effective 4-fermion operator. Indeed, in the low-energy limit, the propagator yields:

$$\Delta(k) = \frac{i}{k^2 - m_h^2} \xrightarrow{k^2 \ll m_h^2} -\frac{i}{m_h^2} \tag{3.5}$$

We have performed the matching by using the equations of motion: such approach takes the name of functional approach. More generally, within this approach, the heavy field is integrated out from the functional integral and the result is the EFT action S_{EFT} that depends only on the light fields:

$$Z = \int \mathcal{D}\Phi\, \mathcal{D}\Psi \mathcal{D}\bar{\Psi}\, e^{iS_{\text{UV}}[\Phi,\Psi,\bar{\Psi}]} = \int \mathcal{D}\Psi \mathcal{D}\bar{\Psi} e^{iS_{\text{EFT}}[\Psi,\bar{\Psi}]}, \tag{3.6}$$

where

$$S_{\text{UV}}[\Phi, \Psi, \bar{\Psi}] = \int d^4x \mathcal{L}_{\text{UV}}[\Phi, \Psi, \bar{\Psi}], \quad S_{\text{EFT}}[\Psi, \bar{\Psi}] = \int d^4x \mathcal{L}_{\text{EFT}}[\Psi, \bar{\Psi}]. \tag{3.7}$$

Conversely, the diagrammatic approach consists of matching a set of amplitudes in both theories and imposing that the two results are the same at energies much lower than m_h. In our case, equating the two amplitudes stemming from the Feynman diagrams in Fig. 3.1, properly expanded in E/m_h, provides an equation for c.
We can generalize the findings of this simple example by stating that the EFT Lagrangian can be expressed as an infinite sum of higher-dimensional operators built out of the light fields:

$$\mathcal{L}_{\text{EFT}} = \mathcal{L}_{\mathcal{D}\leq 4} + \sum_{\mathcal{D}=5}^{\infty} \frac{1}{m_h^{\mathcal{D}-4}} \sum_{i=1}^{n_{\mathcal{D}}} C_i^{(\mathcal{D})} Q_i^{(\mathcal{D})}, \tag{3.8}$$

where here and in the following $\mathcal{D}$ is the mass dimension of the operator Q_i and $n_{\mathcal{D}}$ is the finite number of independent operators with dimension $\mathcal{D}$. $C_i^{(\mathcal{D})}$ is the dimensionless Wilson coefficient associated to the dimension $\mathcal{D}$ operator $Q_i^{(\mathcal{D})}$. By retaining higher terms in k^2/m_h^2, higher-dimensional operators would be generated.

Bottom-Up approach

EFTs can also be a useful tool in the opposite scenario, namely when the full theory is unknown and, therefore, it is constructed based only on symmetry arguments that must be satisfied in order to correctly recover the known low-energy behavior. Indeed, the Lagrangian in eq. (3.8) can be defined without any reference to the complete model, where m_h represents the typical energy scale of the heavy degrees of freedom. In other words, the EFT offers a framework to parametrize a general theory satisfying the assumed symmetries. Moreover, the WCs of the effective operators are free parameters of the theory, to be bound by comparison with experiments, thus they do not emerge from the matching procedure as in the Top-Down approach. This is the philosophy that will be followed within this thesis in the framework of the SMEFT, described in the following section.

3.1 Standard Model Effective Field Theory

The SMEFT is parametrized by adding, to the SM Lagrangian, a series of higher dimension operators constructed with SM fields, that must transform under G_{SM} exactly as in the SM.
The assumption that the Higgs boson transforms as part of an $SU(2)_L$ doublet could be lifted. In such case, the resulting EFT would be the the so-called Higgs Effective Field Theory (HEFT), in which the Goldstones and the physical Higgs boson transform in different representations and are not bound to be a $SU(2)_L$ SM doublet. As a consequence, the electroweak symmetry breaking is not linearly realized in the HEFT framework.

The SMEFT operators are defined using only symmetry arguments: Lorentz invariance, the SM gauge symmetry G_{SM} in eq. (2.1) and, eventually, global symmetries such as baryon and lepton number. In fact, the UV theory must have a local symmetry group that includes G_{SM} as a subgroup. Instead the global symmetries could be approximate symmetries accidentally arising at low energies and, therefore, one can make different assumptions by deciding whether to include them or not. Furthermore, the SMEFT Lagrangian is built on the assumption that no other light degrees of freedom, apart from the SM ones, are present.
The SMEFT Lagrangian can symbolically be decomposed as

$$\mathcal{L}_{\text{SMEFT}}(\Psi, \varphi, A) = \mathcal{L}_{\text{SM}}(\Psi, \varphi, A) + \sum_{\mathcal{D}=5}^{\infty} \sum_{i=1}^{n_{\mathcal{D}}} \frac{C_i^{(\mathcal{D})}}{\Lambda^{\mathcal{D}-4}} Q_i^{(\mathcal{D})}(\Psi, \varphi, A), \tag{3.9}$$

where the same notation as in eq. (3.8) is used and Λ denotes the new heavy BSM scale. Ψ, φ and A symbolically denote the SM fermion, Higgs and gauge fields, respectively.
The SM is the low-energy dimension-four limit of the SMEFT; the order d in which to truncate the series determines the precision of the EFT expansion.
Up to dimension 6 the SMEFT Lagrangian is given by

$$\mathcal{L}_{\text{SMEFT}} = \mathcal{L}_{\text{SM}} + \frac{1}{\Lambda}\mathcal{L}_5 + \frac{1}{\Lambda^2}\mathcal{L}_6 + \mathcal{O}(\Lambda^{-3}), \tag{3.10}$$

where $\mathcal{L}_5$ and $\mathcal{L}_6$ contain all the dimension-five and dimension-six operators, respectively.
There is only one dimension-five operator, called Weinberg operator, which introduces a Majorana mass for left-handed neutrinos. Hence, this operator violates lepton number, which is one of the global symmetries of the SM, and for this reason its effect is very suppressed.
In this thesis, the operators taken into account do not violate lepton and baryon number conservation. Therefore, only operators in $\mathcal{L}_6$ will be considered.
A minimal set of dimension-six operators, namely a basis, is constructed by eliminating the redundant ones applying:

a) *Integration by parts.* The action $S = \int d^4x\mathcal{L}$ is the same for two Lagrangians that differ only for total derivative terms, once it is assumed that all fields vanish at infinity. We can therefore take into account only the operators of one of the two Lagrangians.

b) *Field redefinitions.* According to the LSZ reduction formula, it is possible to perform field redefinitions, reducing the number of operators without modifying physical observables.

c) *Fierz identities and Dirac structure reduction.* These identities are relations among four-fermion operators; the number of the independent ones can, therefore, be reduced ([9]).

The most common minimal set of dimension-six operators in the SMEFT is the Warsaw basis, described in the next paragraph.

Warsaw basis

Assuming one fermion generation, the Warsaw basis contains 59 non-redundant dimension-six operators, conserving baryon and lepton numbers [10]. They are divided into classes according to

their field content in Table 3.1. If all the three fermion generations are included, the number of independent operators increases to 2499, in the most flavour-agnostic scenario.
Operators of class 7 are matrices in the flavour space, namely they have indices $[a, b]$, with $a, b = 1, 2, 3$. In order to preserve the flavour, they must be diagonal, namely $a = b$.
The operators can also be classified as potentially tree-generated (TG) or loop-generated (LG), as in Ref. [11–13], under the assumption of renormalizable and weakly coupled extensions of the SM. Different BSM theories can generate different operators at different orders in the loop expansion of a certain process, hence this strategy allows to know which operators are potentially generated by tree-level matching, hence potentially contributing dominantly to observables. Conversely, if the operators are generated at loop-level in the matching, they are expected to contribute subdominantly, as they would be suppressed by an additional loop factor of, at least, $1/(16\pi^2)$. In the Warsaw basis, there are three classes of LG operators: X^3, $X^2\varphi^2$ and $\Psi^2 X\varphi$, as also stressed in Table 3.1.
In order to reduce the number of free parameters, some flavour assumptions can be taken. A common choice is Minimal Flavour Violation (MFV) hypothesis [14]. The largest flavour-symmetry group of the SM Lagrangian is

$$G_{\text{flavour}} = U(3)^5 = U(3)_l \otimes U(3)_q \otimes U(3)_e \otimes U(3)_u \otimes U(3)_d. \tag{3.11}$$

This symmetry allows independent unitary rotation in flavour space on each of the five fermion fields without modifying the gauge and kinetic terms of the SM Lagrangian. Mathematically,

$$\begin{cases} l_L \xrightarrow{U(3)_l} U_l l_L, & U_l \in U(3)_l \\ q_L \xrightarrow{U(3)_q} U_q q_L, & U_q \in U(3)_q \\ e_R \xrightarrow{U(3)_e} U_e e_R, & U_e \in U(3)_e \\ u_R \xrightarrow{U(3)_u} U_u u_R, & U_u \in U(3)_u \\ d_R \xrightarrow{U(3)_d} U_d d_R, & U_d \in U(3)_d \end{cases} . \tag{3.12}$$

The MFV hypothesis assumes that the Yukawa sector of the SM Lagrangian in eq. (2.35) is the only source of G_{flavour} breaking. To formally restore the symmetry, the Yukawa matrices can be promoted to spurion fields such that, under G_{flavour}, they transform as

$$\begin{cases} Y_e \xrightarrow{U(3)^5} U_l Y_e U_e^\dagger \\ Y_u \xrightarrow{U(3)^5} U_q Y_u U_u^\dagger \\ Y_d \xrightarrow{U(3)^5} U_q Y_d U_d^\dagger \end{cases} . \tag{3.13}$$

The operators in classes 5 and 6 of Table 3.1 connect left-handed and right-handed fermions. In order to preserve the symmetry G_{flavour}, a Yukawa spurion must be inserted. In MFV, operators that contain Yukawa spurions are suppressed by Yukawa eigenvalues and CKM factors.
Finally, the allowed 4-fermion operator structures that are invariant under the $U(3)^5$ symmetry (3.11) are $(\bar{L}L)(\bar{L}L)$, $(\bar{R}R)(\bar{R}R)$ and $(\bar{L}L)(\bar{R}R)$. There are two independent WCs associated to, for example, $\mathcal{O}_{ll}$ because there are two ways in which its flavour indices can be contracted: $(\bar{l}_p\gamma_\mu l_p)(\bar{l}_r\gamma^\mu l_r)$ and $(\bar{l}_p\gamma_\mu l_r)(\bar{l}_r\gamma^\mu l_p)$. Therefore, if i, j, k, l are flavour indices, we have the following structure for the WCs associated to $\mathcal{O}_{ll}$:

$$C_{ll}^{i,j,k,l}\mathcal{O}_{ll}^{i,j,k,l} = (C_1\delta_{ij}\delta_{kl} + C_2\delta_{il}\delta_{jk})\mathcal{O}_{ll}^{i,j,k,l} = \\ = (C_1 + C_2)\mathcal{O}_{ll}^{i,i,i,i} + C_1\mathcal{O}_{ll}^{i,i,j,j} + C_2\mathcal{O}_{ll}^{i,j,j,i} \tag{3.14}$$

As a consequence, the two independent WCs associated to $\mathcal{O}_{ll}$ are C_1 and C_2 and the following relations yield:

$$\begin{cases} C_1 + C_2 = C_{ll}^{i,i,i,i} \\ C_1 = C_{ll}^{i,i,j,j} \\ C_2 = C_{ll}^{i,j,j,i} \end{cases} \qquad \text{where } i,j = 1,2,3 \text{ and } i \neq j. \tag{3.15}$$

There is instead only one possible way to contract, for example, the $\mathcal{O}_{lq}^{(3)}$ flavour indices such that the invariance under the $U(3)^5$ symmetry is preserved: $(\bar{l}_p\gamma_\mu\tau^I l_p)(\bar{q}_r\gamma^\mu\tau^I q_r)$. Therefore, there is only one independent WC: $C_{lq}^{(3),i,i,j,j}$ where $i,j = 1,2,3$.

$1: X^3$ (LG)	
$\mathcal{O}_G$	$f^{ABC} G_\mu^{A\nu} G_\nu^{B\rho} G_\rho^{C\mu}$
$\mathcal{O}_{\tilde{G}}$	$f^{ABC} \tilde{G}_\mu^{A\nu} G_\nu^{B\rho} G_\rho^{C\mu}$
$\mathcal{O}_W$	$\varepsilon^{IJK} W_\mu^{I\nu} W_\nu^{J\rho} W_\rho^{K\mu}$
$\mathcal{O}_{\tilde{W}}$	$\varepsilon^{IJK} \tilde{W}_\mu^{I\nu} W_\nu^{J\rho} W_\rho^{K\mu}$

$2: \varphi^6$	
$\mathcal{O}_\varphi$	$(\varphi^\dagger \varphi)^3$

$3: \varphi^4 D^2$	
$\mathcal{O}_{\varphi\Box}$	$(\varphi^\dagger \varphi)\Box(\varphi^\dagger \varphi)$
$\mathcal{O}_{\varphi D}$	$(\varphi^\dagger D^\mu \varphi)^* (\varphi^\dagger D_\mu \varphi)$

$5: \psi^2 \varphi^3$	
$\mathcal{O}_{e\varphi}$	$(\varphi^\dagger \varphi)(\bar{l}_p e_r \varphi)$
$\mathcal{O}_{u\varphi}$	$(\varphi^\dagger \varphi)(\bar{q}_p u_r \tilde{\varphi})$
$\mathcal{O}_{d\varphi}$	$(\varphi^\dagger \varphi)(\bar{q}_p d_r \varphi)$

$4: X^2 \varphi^2$ (LG)	
$\mathcal{O}_{\varphi G}$	$(\varphi^\dagger \varphi) G^A_{\mu\nu} G^{A\mu\nu}$
$\mathcal{O}_{\varphi \tilde{G}}$	$(\varphi^\dagger \varphi) \tilde{G}^A_{\mu\nu} G^{A\mu\nu}$
$\mathcal{O}_{\varphi W}$	$(\varphi^\dagger \varphi) W^I_{\mu\nu} W^{I\mu\nu}$
$\mathcal{O}_{\varphi \tilde{W}}$	$(\varphi^\dagger \varphi) \tilde{W}^I_{\mu\nu} W^{I\mu\nu}$
$\mathcal{O}_{\varphi B}$	$(\varphi^\dagger \varphi) B_{\mu\nu} B^{\mu\nu}$
$\mathcal{O}_{\varphi \tilde{B}}$	$(\varphi^\dagger \varphi) \tilde{B}_{\mu\nu} B^{\mu\nu}$
$\mathcal{O}_{\varphi WB}$	$(\varphi^\dagger \tau^I \varphi) W^I_{\mu\nu} B^{\mu\nu}$
$\mathcal{O}_{\varphi \tilde{W}B}$	$(\varphi^\dagger \tau^I \varphi) \tilde{W}^I_{\mu\nu} B^{\mu\nu}$

$6: \psi^2 X \phi$ (LG)	
$\mathcal{O}_{eW}$	$(\bar{l}_p \sigma^{\mu\nu} e_r) \tau^I \varphi W^I_{\mu\nu}$
$\mathcal{O}_{eB}$	$(\bar{l}_p \sigma^{\mu\nu} e_r) \varphi B_{\mu\nu}$
$\mathcal{O}_{uG}$	$(\bar{q}_p T^A \sigma^{\mu\nu} u_r) \tilde{\varphi} G^A_{\mu\nu}$
$\mathcal{O}_{uW}$	$(\bar{q}_p \sigma^{\mu\nu} u_r) \tau^I \tilde{\varphi} W^I_{\mu\nu}$
$\mathcal{O}_{uB}$	$(\bar{q}_p \sigma^{\mu\nu} u_r) \tilde{\varphi} B_{\mu\nu}$
$\mathcal{O}_{dG}$	$(\bar{q}_p T^A \sigma^{\mu\nu} d_r) \varphi G^A_{\mu\nu}$
$\mathcal{O}_{dW}$	$(\bar{q}_p \sigma^{\mu\nu} d_r) \tau^I \varphi W^I_{\mu\nu}$
$\mathcal{O}_{dB}$	$(\bar{q}_p \sigma^{\mu\nu} d_r) \varphi B_{\mu\nu}$

$7: \psi^2 \varphi^2 D$	
$\mathcal{O}_{\varphi l(1)}$	$(\varphi^\dagger i \overleftrightarrow{D}_\mu \varphi)(\bar{l}_p \gamma^\mu l_r)$
$\mathcal{O}_{\varphi l(3)}$	$(\varphi^\dagger i \overleftrightarrow{D}^I_\mu \varphi)(\bar{l}_p \tau^I \gamma^\mu l_r)$
$\mathcal{O}_{\varphi e}$	$(\varphi^\dagger i \overleftrightarrow{D}_\mu \varphi)(\bar{e}_p \gamma^\mu e_r)$
$\mathcal{O}_{\varphi q(1)}$	$(\varphi^\dagger i \overleftrightarrow{D}_\mu \varphi)(\bar{q}_p \gamma^\mu q_r)$
$\mathcal{O}_{\varphi q(3)}$	$(\varphi^\dagger i \overleftrightarrow{D}^I_\mu \varphi)(\bar{q}_p \tau^I \gamma^\mu q_r)$
$\mathcal{O}_{\varphi u}$	$(\varphi^\dagger i \overleftrightarrow{D}_\mu \varphi)(\bar{u}_p \gamma^\mu u_r)$
$\mathcal{O}_{\varphi d}$	$(\varphi^\dagger i \overleftrightarrow{D}_\mu \varphi)(\bar{d}_p \gamma^\mu d_r)$
$\mathcal{O}_{\varphi ud}$	$(\tilde{\varphi}^\dagger i D_\mu \varphi)(\bar{u}_p \gamma^\mu d_r)$

$8: (\bar{L}L)(\bar{L}L)$	
$\mathcal{O}_{ll}$	$(\bar{l}_p \gamma_\mu l_r)(\bar{l}_s \gamma^\mu l_t)$
$\mathcal{O}_{qq(1)}$	$(\bar{q}_p \gamma_\mu q_r)(\bar{q}_s \gamma^\mu q_t)$
$\mathcal{O}_{qq(3)}$	$(\bar{q}_p \gamma_\mu \tau^I q_r)(\bar{q}_s \gamma^\mu \tau^I q_t)$
$\mathcal{O}_{lq(1)}$	$(\bar{l}_p \gamma_\mu l_r)(\bar{q}_s \gamma^\mu q_t)$
$\mathcal{O}_{lq(3)}$	$(\bar{l}_p \gamma_\mu \tau^I l_r)(\bar{q}_s \gamma^\mu \tau^I q_t)$

$8: (\bar{R}R)(\bar{R}R)$	
$\mathcal{O}_{ee}$	$(\bar{e}_p \gamma_\mu e_r)(\bar{e}_s \gamma^\mu e_t)$
$\mathcal{O}_{uu}$	$(\bar{u}_p \gamma_\mu u_r)(\bar{u}_s \gamma^\mu u_t)$
$\mathcal{O}_{dd}$	$(\bar{d}_p \gamma_\mu d_r)(\bar{d}_s \gamma^\mu d_t)$
$\mathcal{O}_{eu}$	$(\bar{e}_p \gamma_\mu e_r)(\bar{u}_s \gamma^\mu u_t)$
$\mathcal{O}_{ed}$	$(\bar{e}_p \gamma_\mu e_r)(\bar{d}_s \gamma^\mu d_t)$
$\mathcal{O}_{ud(1)}$	$(\bar{u}_p \gamma_\mu u_r)(\bar{d}_s \gamma^\mu d_t)$
$\mathcal{O}_{ud(8)}$	$(\bar{u}_p \gamma_\mu T^A u_r)(\bar{d}_s \gamma^\mu T^A d_t)$

$8: (\bar{L}L)(\bar{R}R)$	
$\mathcal{O}_{le}$	$(\bar{l}_p \gamma_\mu l_r)(\bar{e}_s \gamma^\mu e_t)$
$\mathcal{O}_{lu}$	$(\bar{l}_p \gamma_\mu l_r)(\bar{u}_s \gamma^\mu u_t)$
$\mathcal{O}_{ld}$	$(\bar{l}_p \gamma_\mu l_r)(\bar{d}_s \gamma^\mu d_t)$
$\mathcal{O}_{qe}$	$(\bar{q}_p \gamma_\mu q_r)(\bar{e}_s \gamma^\mu e_t)$
$\mathcal{O}_{qu(1)}$	$(\bar{q}_p \gamma_\mu q_r)(\bar{u}_s \gamma^\mu u_t)$
$\mathcal{O}_{qu(8)}$	$(\bar{q}_p \gamma_\mu T^A q_r)(\bar{u}_s \gamma^\mu T^A u_t)$
$\mathcal{O}_{qd(1)}$	$(\bar{q}_p \gamma_\mu q_r)(\bar{d}_s \gamma^\mu d_t)$
$\mathcal{O}_{qd(8)}$	$(\bar{q}_p \gamma_\mu T^A q_r)(\bar{d}_s \gamma^\mu T^A d_t)$

$8: (\bar{L}R)(\bar{R}L)$	
$\mathcal{O}_{ledq}$	$(\bar{l}_p e_r)(\bar{d}_s q_t)$

$8: (\bar{L}R)(\bar{L}R)$	
$\mathcal{O}_{quqd(1)}$	$(\bar{q}^j_p u_r)\varepsilon_{jk}(\bar{q}^k_s d_t)$
$\mathcal{O}_{quqd(8)}$	$(\bar{q}^j_p T^A u_r)\varepsilon_{jk}(\bar{q}^k_s T^A d_t)$
$\mathcal{O}_{lequ(1)}$	$(\bar{l}^j_p e_r)\varepsilon_{jk}(\bar{q}^k_s u_t)$
$\mathcal{O}_{lequ(3)}$	$(\bar{l}^j_p \sigma_{\mu\nu} e_r)\varepsilon_{jk}(\bar{q}^k_s \sigma^{\mu\nu} u_t)$

Table 3.1: The 59 independent dimension-six operators built from SM fields which preserve baryon and lepton number from [15]. p, r, s, t are fermion flavor indices, j, k are indices in the fundamental representation of $\mathrm{SU}(2)_\mathrm{L}$, I, J, K (A, B, C) are indices in the adjoint representation of $\mathrm{SU}(2)_\mathrm{L}$ ($\mathrm{SU}(3)_\mathrm{C}$) and $\mu, \nu \ldots$ are Lorentz indices. The contraction of indices in the fundamental representation of $\mathrm{SU}(3)_\mathrm{C}$ is left implicit.

Chapter 4

HS+VBF leading-order cross section at the circular colliders

Future colliders offer promising prospects in unveiling NP and finally solve the SM shortcomings. Most likely, the next collider to be built will be an electron-positron collider, whose clean environment will bring an unprecedented precision for many SM parameters, providing a powerful stress test for the theory itself. A deviation from the SM expectation could be the first indirect sign of BSM physics.
Among the various projects, the Future Circular Collider (FCC) is a future underground circular collider, planned with a circumference of 90.7 km, that could follow the Large Hadron Collider (LHC) at CERN from the late 2040s [2]. For the first 15 years, the FCC would be an electron-positron collider (FCC-ee), evolving in the following decades to a hadron collider (FCC-hh).
There are two production mechanisms for single Higgs production in association with two electron neutrinos. The first is the Higgsstrahlung (HS), in which a virtual Z boson decays into a Higgs boson and a Z boson (which following decays into two electron neutrinos), as in the left diagram of Fig. 4.2. The cross section of this s-channel process has a maximum around $\sqrt{s} = 240$ GeV. At higher energies, the cross section decreases with the inverse of the squared centre-of-mass (CM) energy s of the e^+e^- system.
The second production channel instead the Vector Boson Fusion (VBF), a t-channel in which both the electron and the positron emit a W boson. The two W bosons then fuse into a Higgs boson, as shown in the diagram on the right of Figure 4.2. Its cross section grows with the logarithm of s and, therefore, the VBF is expected to become the predominant channel at high energies, far beyond $\sqrt{s} = 209$ GeV, the maximum reached by the Large Electron-Positron Collider (LEP), as Figure 4.1 shows.

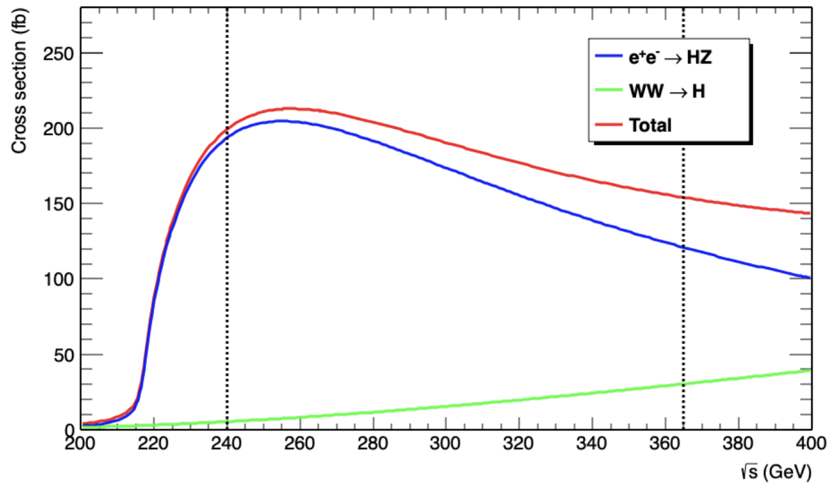

Figure 4.1: Cross section trends for the two separated subprocesses (blue for the HS and green for the VBF) and for the total process (red) [16]. The HS cross section has a maximum at about $\sqrt{s} = 240$ GeV and then decreases with the inverse of s. The VBF cross section instead grows with the logarithm of s.

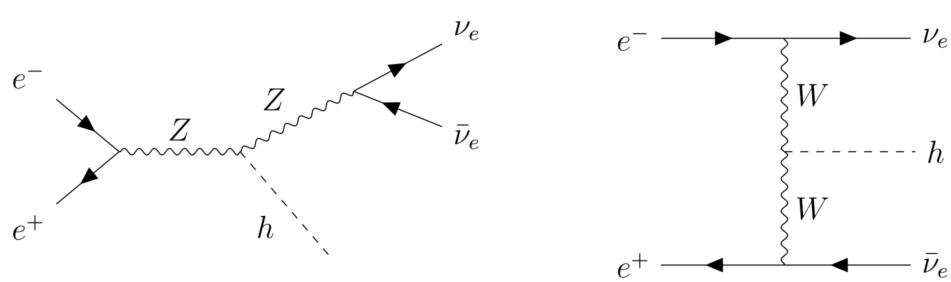

Figure 4.2: Lowest-order diagrams for $e^+e^- \to \nu_e\bar{\nu}_e h$.

FCC-ee measurements relevant for single Higgs production are planned two different values for the center-of-mass energy: at $\sqrt{s}$ =240 GeV, where the optimal event rate and the best signal-to-background ratio for the HS are achieved, and at $\sqrt{s}$ =350 or 365 GeV.
In the following, a detailed analysis is performed to quantify how important the VBF is relative to the HS at a CM energy of 350 GeV, at LO in the SMEFT. Moreover, we discuss how large the interference between the two production mechanisms could be.

4.1 Identification of relevant dimension-six SMEFT operators

Dimension-six operators can contribute to the $e^+e^- \to \nu_e\bar{\nu}_e h$ cross section, both by shifting SM couplings with a term proportional to their corresponding Wilson coefficients and by creating new interaction vertices. Since we truncate the Lagrangian at dimension-six, each Feynman diagram contains at most one NP vertex, since multiple insertions would be of higher order. Furthermore, the amplitudes are computed in the limit of massless fermions.

Consistently, the cross section is truncated up to linear terms in $1/\Lambda^2$, where Λ denotes the NP scale as in Chapter 3, and it can be written schematically as:

$$\begin{aligned}
\sigma_{\text{VBF+HS}} &= \int d\Phi_3 |M_{\text{VBF}} + M_{\text{HS}}|^2 \\
&= \int d\Phi_3 \Big(|M^{\text{SM}}_{\text{VBF}}|^2 + 2\,\text{Re}(M^{\text{SM}*}_{\text{VBF}} M^{\text{NP}}_{\text{VBF}}) \Big) && \text{Pure VBF cross section} \\
&+ \int d\Phi_3 \Big(2\,\text{Re}(M^{\text{SM}*}_{\text{VBF}} M^{\text{SM}}_{\text{HS}} + M^{\text{NP}*}_{\text{VBF}} M^{\text{SM}}_{\text{HS}} + M^{\text{SM}*}_{\text{VBF}} M^{\text{NP}}_{\text{HS}}) \Big) && \text{VBF-HS interference} \\
&+ \int d\Phi_3 \Big(|M^{\text{SM}}_{\text{HS}}|^2 + 2\,\text{Re}(M^{\text{SM}*}_{\text{HS}} M^{\text{NP}}_{\text{HS}}) \Big). && \text{Pure HS cross section}
\end{aligned}$$

$d\Phi_3$ symbolizes the phase space element for the three particles in the final state and NP denotes the SMEFT contribution linear in $1/\Lambda^2$.

The operators contributing to the tree-level cross section $\sigma_{\text{VBF+HS}}$ could, in principle, be 12: $\mathcal{O}_{\varphi W}$, $\mathcal{O}_{eW}$, $\mathcal{O}^{(3)}_{\varphi l}$, $\mathcal{O}_{eB}$, $\mathcal{O}_{\varphi B}$, $\mathcal{O}_{\varphi WB}$, $\mathcal{O}^{(1)}_{\varphi l}$, $\mathcal{O}_{\varphi D}$, $\mathcal{O}_{\varphi\Box}$, $\mathcal{O}_{\varphi e}$, $\mathcal{O}_{\varphi}$ and $\mathcal{O}_{e\varphi}$. However, only 7 operators contribute, as explained in the following in detail. The operators $\mathcal{O}_{e\varphi}$, $\mathcal{O}_{eW}$ and $\mathcal{O}_{eB}$ are excluded under the MFV assumption, as explained in Sec. 3.1. They involve fermions of the first and second generations and, therefore, in the massless-fermion limit, they are neglected.
Even if the MFV assumption was not taken into account, $\mathcal{O}_{eW}$ and $\mathcal{O}_{eB}$ could still be neglected. The first contributes to the VBF vertices involving a W boson and a fermionic current, whereas the second contributes to the HS vertices with a photon or a Z boson and the electron current.

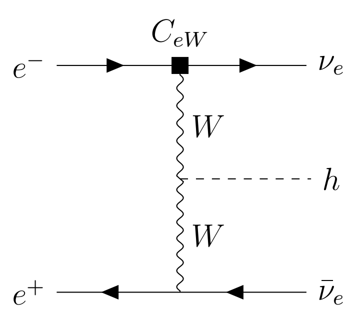

Figure 4.3: VBF diagram with a contribution from the SMEFT operator $\mathcal{O}_{eW}$ represented with the black square dot.

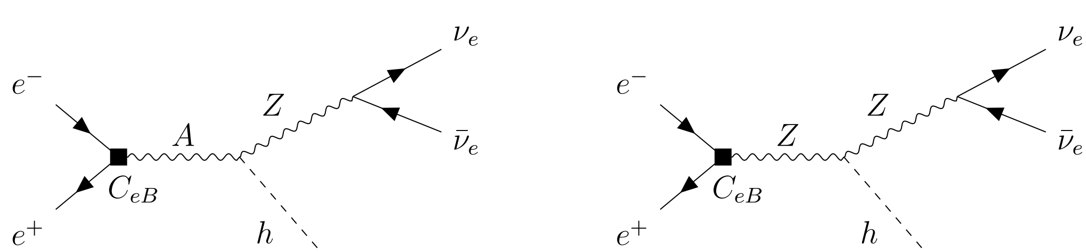

Figure 4.4: HS diagrams with the photon propagator on the left and the Z boson propagator on the right. The black square dot represents the SMEFT operator $\mathcal{O}_{eB}$.

$\mathcal{O}_{eW}$ and $\mathcal{O}_{eB}$ flip the fermion chirality because they connect a left-handed lepton doublet to a right-handed electron. In contrast, the SM operators that contribute to these vertices are proportional to γ^μ, if the propagator is a photon, or to a mixture of γ^μ and $\gamma^\mu\gamma_5$ if the propagator is instead a Z or a W boson. In both cases, the SM currents do not flip chirality:

$$\bar{\Psi}_L\gamma^\mu\Psi_R = 0, \quad \bar{\Psi}_L\gamma^\mu\gamma_5\Psi_R = 0.$$

Since we are working in the limit of massless fermions, chirality coincides with helicity. In $\sigma_{\text{VBF+HS}}$, terms proportional to the Wilson coefficients C_{eW} or C_{eB} give zero because two orthogonal helicity states are multiplied. $\mathcal{O}_\varphi$ is neglected as well since it contributes to vertices with two neutral Goldstones G_0 and one Higgs boson h. Since it has been imposed that at most one NP vertex can be present in each diagram, every time that $\mathcal{O}_\varphi$ contributes to the square vertex in Figure 4.5, there is a SM vertex, represented by the circle, mediated by a Yukawa interaction, proportional to the fermion mass.

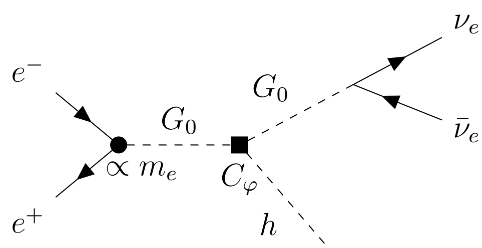

Figure 4.5: HS diagram where the propagator is the neutral Goldstone G_0. The black dot represents a SM vertex proportional to the electron mass. The SMEFT operator $\mathcal{O}_\varphi$ is instead represented with the black square dot.

In the massless-fermion limit, the amplitude of every diagram containing $\mathcal{O}_\varphi$ vanishes.
Finally, we neglect $\mathcal{O}^{(1)}_{\varphi l}$ because it does not contribute to the cross section. When the term of the modulus square of the amplitude proportional to $C^{(1)}_{\varphi l}$ is integrated over the phase space for the final state particles, it gives a vanishing contribution to the SM cross section.
To summarize, the set of operators we consider in this analysis is, therefore: $\{\mathcal{O}_{\varphi W}$, $\mathcal{O}^{(3)}_{\varphi l}$, $\mathcal{O}_{\varphi B}$, $\mathcal{O}_{\varphi WB}$, $\mathcal{O}_{\varphi D}$, $\mathcal{O}_{\varphi\Box}$, $\mathcal{O}_{\varphi e}\}$.

4.2 Quantifiation of truncation effects on the cross section

In this section, we analyze the relative size of the quadratic contribution of the cross section, proportional to $1/\Lambda^4$, compared to the linear contribution in $1/\Lambda^2$, at a CM energy of $\sqrt{s}$ =350 GeV. The squared amplitude of $e^-e^+ \to h\nu_e\bar{\nu}_e$ is computed with `GoSam` [7]. The integration over the phase space to obtain the cross section is performed with the Monte Carlo generator `Whizard` [17]. This analysis is performed by independently varying one WC from each class of the Warsaw basis relevant for our process, namely $C_{\varphi D}$, $C_{\varphi W}$ and $C_{\varphi e}$. The least stringent bounds from LHC measurements used for our analysis are provided in Table 4.1.
The SMEFT cross section can be parametrize as

$$\sigma_{\text{SMEFT}} = \sigma_{\text{SM}} + \sum_i C_i\sigma_i + \sum_{i,j} C_iC_j\sigma_{ij}. \tag{4.1}$$

Each WC C_i in eq. (4.1) already includes the factor $1/\Lambda^2$.

Wilson coefficient	Lower bound ($\cdot 10^{-6}$ GeV^{-2})	Upper bound ($\cdot 10^{-6}$ GeV^{-2})
$C_{\varphi W}$	-0.273	0.707
$C_{\varphi l}^{(3)}$	-0.136	0.064
$C_{\varphi B}$	-0.310	0.573
$C_{\varphi WB}$	-0.525	0.504
$C_{\varphi D}$	-1.063	1.149
$C_{\varphi \Box}$	-1.715	1.879
$C_{\varphi e}$	-0.583	0.527

Table 4.1: Experimental bounds on Wilson coefficients from LHC measurements, taken from [18] and [19].

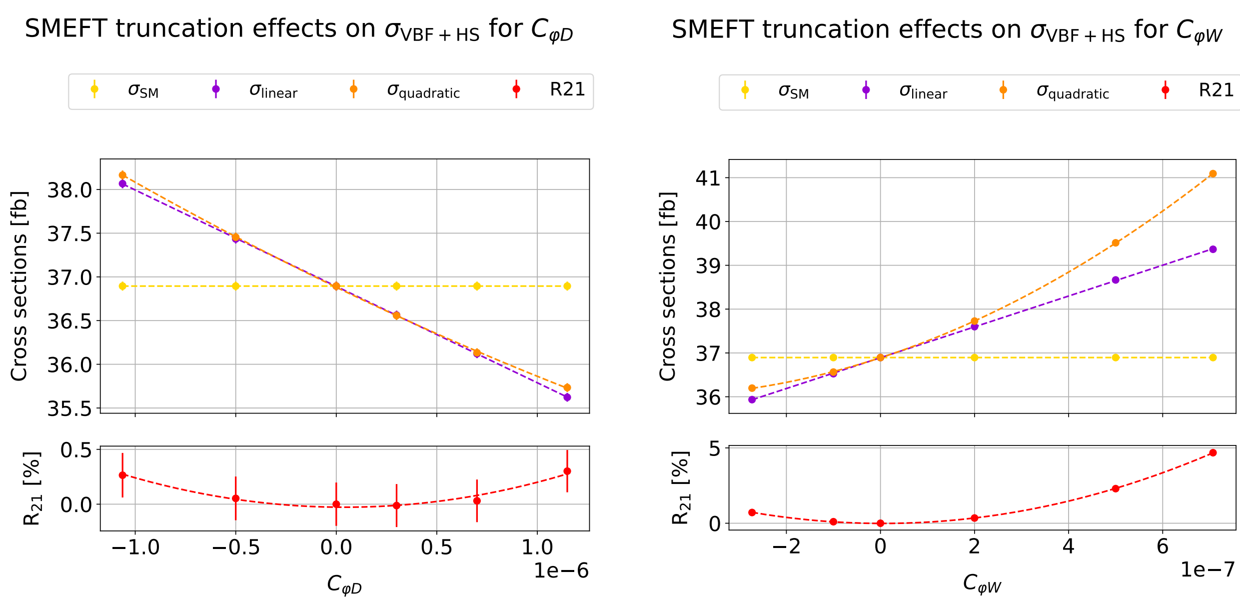

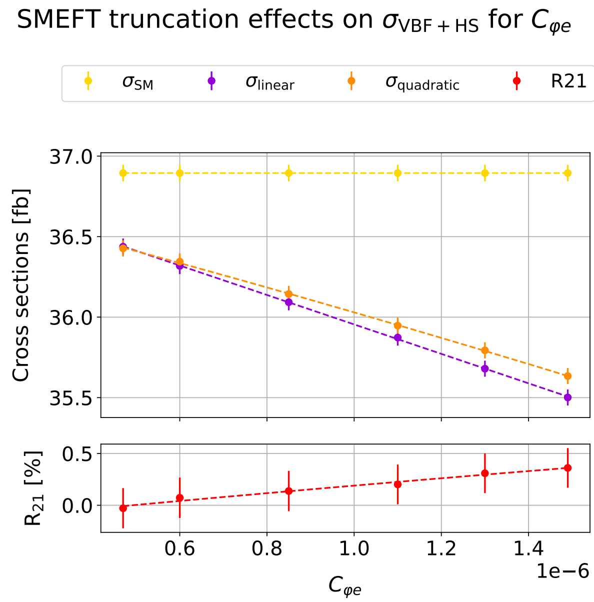

Figure 4.6: Plots with cross sections trends for different truncation orders in $1/\Lambda^2$ and for different WCs. In the bottom R_{21}= $(\sigma_{\mathrm{quad}} - \sigma_{\mathrm{linear}})/\sigma_{\mathrm{linear}}$ represents how the quadratic cross section differs from the linear one, in percentage.

In Figure 4.6 the WCs have been varied within the LHC bounds in Table 4.1.
We observe that $\sigma_{\mathrm{quadratic}}$ does not differ significantly from σ_{linear} or, in other words, their difference, quantified by R_{21}, is very small in the whole range of the considered WCs. The projected WCs bounds for the FCC are much more stringent [18]: as a consequence, we expect R_{21} to be very close to zero. We conclude that the quadratic terms are subdominant, hence we will consistently truncate our results up to the linear term in $1/\Lambda^2$.

4.3 Quantifying VBF-HS interference and VBF dominance at 350 GeV in LO SMEFT

The linear SMEFT cross section can be parametrized as the SM one plus seven linear terms, each of them proportional to one of the WCs of our SMEFT basis at the end of Sec. 4.1. This parameterization holds for both the total cross section and the two individual channels:

$$\sigma^{\mathrm{TOT}}_{\mathrm{SMEFT}} - \sigma^{\mathrm{TOT}}_{\mathrm{SM}} = \sum_{i=1}^{7} C_i A_i^{\mathrm{TOT}} \tag{4.2}$$

$$\sigma^{\mathrm{HS}}_{\mathrm{SMEFT}} - \sigma^{\mathrm{HS}}_{\mathrm{SM}} = \sum_{i=1}^{7} C_i A_i^{\mathrm{HS}} \tag{4.3}$$

$$\sigma^{\mathrm{VBF}}_{\mathrm{SMEFT}} - \sigma^{\mathrm{VBF}}_{\mathrm{SM}} = \sum_{i=1}^{7} C_i A_i^{\mathrm{VBF}} \tag{4.4}$$

The SMEFT cross sections have been computed for randomly chosen values of the seven WCs within the interval $(-10^{-3}, 10^{-3}) \times \mathrm{GeV}^{-2}$.

The A_i coefficients have been computed as

$$A_i = \frac{\sigma_{\text{SMEFT}} - \sigma_{SM}}{C_i} \tag{4.5}$$

with errors

$$\Delta(A_i) = \frac{\sqrt{\Delta(\sigma_{\text{SMEFT}})^2 + \Delta(\sigma_{\text{SM}})^2}}{|C_i|} \tag{4.6}$$

by considering only one WC at a time.
The WCs are $C_1 = C_{\varphi W}$, $C_2 = C_{\varphi l}^{(3)}$, $C_3 = C_{\varphi B}$, $C_4 = C_{\varphi WB}$, $C_5 = C_{\varphi D}$, $C_6 = C_{\varphi \Box}$ and $C_7 = C_{\varphi e}$. The correspondent A_i coefficients and their errors can be found in Tables 4.2.

A_i^{TOT}	$(A_i \pm \Delta(A_i))(\text{GeV}^2)$
A_1^{TOT}	$(348 \pm 4) \cdot 10^4$
A_2^{TOT}	$(2240 \pm 5) \cdot 10^3$
A_3^{TOT}	$(191 \pm 2) \cdot 10^4$
A_4^{TOT}	$(2974 \pm 7) \cdot 10^3$
A_5^{TOT}	$(-1114 \pm 6) \cdot 10^3$
A_6^{TOT}	$(4473 \pm 7) \cdot 10^3$
A_7^{TOT}	$(-906 \pm 2) \cdot 10^3$

A_i^{HS}	$(A_i \pm \Delta(A_i))(\text{GeV}^2)$
A_1^{HS}	$(686 \pm 1) \cdot 10^4$
A_2^{HS}	$(581 \pm 2) \cdot 10^3$
A_3^{HS}	$(121 \pm 1) \cdot 10^4$
A_4^{HS}	$(3068 \pm 4) \cdot 10^3$
A_5^{HS}	$(3078 \pm 6) \cdot 10^3$
A_6^{HS}	$(970 \pm 1) \cdot 10^3$
A_7^{HS}	$(-878 \pm 1) \cdot 10^3$

A_i^{VBF}	$(A_i \pm \Delta(A_i))(\text{GeV}^2)$
A_1^{VBF}	$(-109 \pm 7) \cdot 10^4$
A_2^{VBF}	$(1831 \pm 3) \cdot 10^3$
A_3^{VBF}	$(-226 \pm 2) \cdot 10^3$
A_4^{VBF}	$(-232 \pm 2) \cdot 10^2$
A_5^{VBF}	$(-908 \pm 1) \cdot 10^3$
A_6^{VBF}	$(3670 \pm 6) \cdot 10^3$
A_7^{VBF}	$(738 \pm 8) \cdot 10$

Table 4.2: A_i coefficients and their errors for the total cross section (TOT) and for the two individual processes (HS and VBF).

We want to quantify how large the interference between the HS and the VBF processes is at $\sqrt{s} = 350$ GeV. We first obtain the SM cross section:

$$\sigma_{\text{SM}}^{\text{TOT}} = (36.89 \pm 0.05)\text{fb}, \qquad \sigma_{\text{SM}}^{\text{HS}} = (8.48 \pm 0.01)\text{fb}, \qquad \sigma_{\text{SM}}^{\text{VBF}} = (30.40 \pm 0.05)\text{fb}.$$

The interference contribution, in percentage, with respect to the VBF cross section and the total one is:

$$I_{\text{SM}} = \left| \frac{\sigma_{\text{SM}}^{\text{TOT}} - \sigma_{\text{SM}}^{\text{HS}} - \sigma_{\text{SM}}^{\text{VBF}}}{\sigma_{\text{SM}}^{\text{VBF}}} \right| \cdot 100 = (6.5 \pm 0.2)\% \tag{4.7}$$

$$Y_{\text{SM}} = \left| \frac{\sigma_{\text{SM}}^{\text{TOT}} - \sigma_{\text{SM}}^{\text{HS}} - \sigma_{\text{SM}}^{\text{VBF}}}{\sigma_{\text{SM}}^{\text{TOT}}} \right| \cdot 100 = (5.4 \pm 0.2)\%. \tag{4.8}$$

The SM interference never exceeds few percent of the total amplitude. We aim to understand if the same result holds also in the SMEFT.
In order to do that, we sample 1000 randomly chosen parameter points within the bounds in Table 4.1 and, for each set of the 7 WCs, we compute the quantities I and Y, defined as:

$$I = \left| \frac{\sigma_{\text{SMEFT}}^{\text{TOT}} - \sigma_{\text{SMEFT}}^{\text{HS}} - \sigma_{\text{SMEFT}}^{\text{VBF}}}{\sigma_{\text{SMEFT}}^{\text{VBF}}} \right| \quad \text{and} \quad Y = \left| \frac{\sigma_{\text{SMEFT}}^{\text{TOT}} - \sigma_{\text{SMEFT}}^{\text{HS}} - \sigma_{\text{SMEFT}}^{\text{VBF}}}{\sigma_{\text{SMEFT}}^{\text{TOT}}} \right| \tag{4.9}$$

The distributions of I and Y for the 1000 points are represented in the histograms in Figure 4.7.

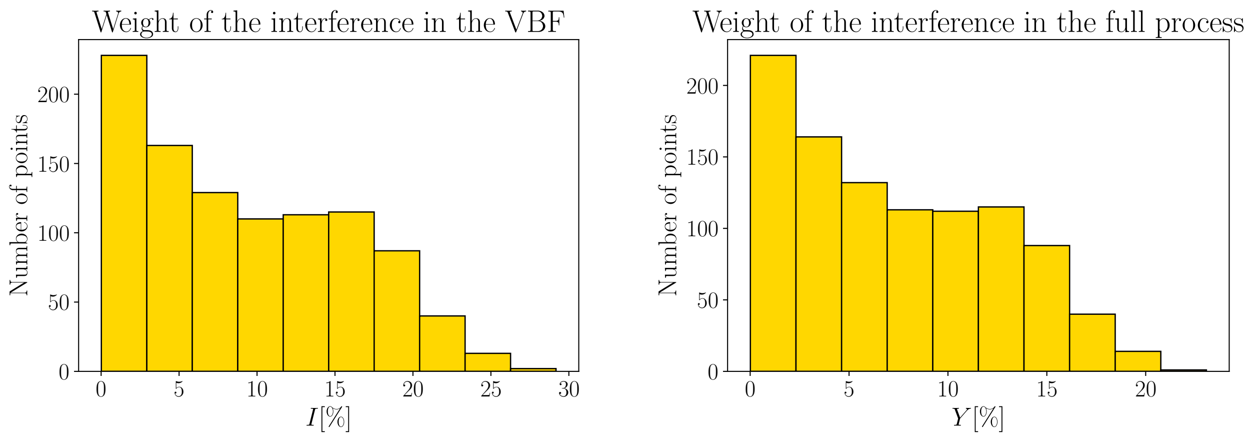

Figure 4.7: Histograms representing the distributions of I and Y, as defined in eq. (4.9).

Figure 4.7 shows that, for certain combinations of WCs, the interference contribution can exceed 20% of either the VBF or the total cross section. These results demonstrate that, within the SMEFT framework, the interference between HS and VBF can not always be neglected.
Nevertheless, the interference starts playing a more important role for less frequent combinations of WCs, namely the graph is decreasing towards increasing I, Y.
Moreover, the histogram I on the left of Figure 4.7 shows a trend similar to that of Y, on the right. As a consequence, one can expect the VBF process to be the dominant production mechanism at $\sqrt{s} = 350$ GeV.
In order to verify this claim, we define the quantities A, B to quantify the relative importance of the two production channels:

$$A = \frac{\sigma^{\text{VBF}}_{\text{SMEFT}}}{\sigma^{\text{TOT}}_{\text{SMEFT}}} \qquad \text{and} \qquad B = \frac{\sigma^{\text{HS}}_{\text{SMEFT}}}{\sigma^{\text{TOT}}_{\text{SMEFT}}}, \tag{4.10}$$

whose histograms are reported in Figure 4.8.

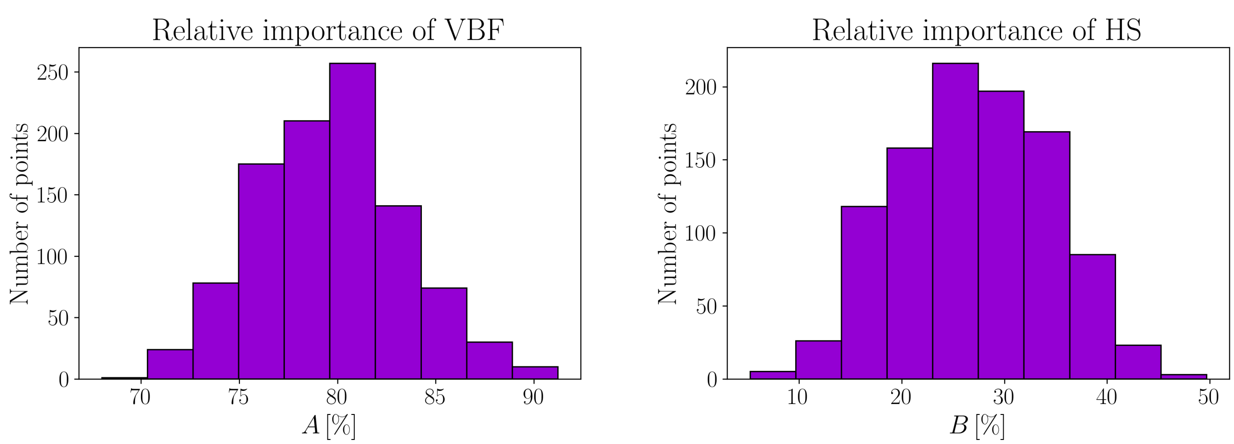

Figure 4.8: Histograms representing the distributions of A and B, as defined in eq. (4.10).

We can therefore conclude that, at the CM energy $\sqrt{s} = 350$ GeV at which we are studying the process $e^+e^- \to \nu_e\bar{\nu}_e h$, the VBF is the dominant channel. For this reason, as a first step of our analysis, we focus on the VBF process, potentially leaving the whole process as a subsequent step.

Chapter 5

Operator basis and NLO effects of SMEFT operators in VBF

In this section, we describe in detail the VBF production channel, discussing which operators we consider in our analysis.
HS and VBF can be distinguished based on the spinor structures of the fermionic currents appearing in the amplitude, as in [4]. In other words, the HS involves lepton-lepton and neutrino-neutrino currents, whereas the VBF contains only lepton-neutrino currents. This distinction is obvious at tree-level. We mention that, at loop level, there are diagrams which involve only neutral current, hence in the categorization we adopt are labelled as HS, but do not involve any internal Z boson, as the one in Fig. 5.1:

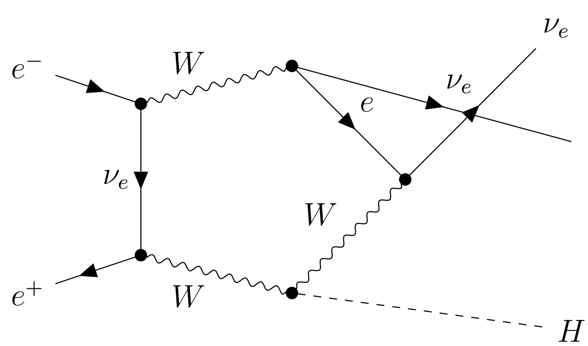

Figure 5.1: NLO HS subprocess with no internal Z boson.

We recall that both the CKM and the PMNS matrices are set to be equal to the identity. As a consequence, flavour-changing transitions are neglected and neutrinos are assumed to be massless. The SMEFT basis of non-parity violating dimension-6 operators contributing to this process includes classes 2,3,7 and some of the 4-fermion operators of class 8, cf. [15]. Classes 5 and 6 are neglected because of the MFV hypothesis, as explained in Sect. 4.1. LG operators of classes 1 and 4 are not included in loop diagrams because they are suppressed as explained in 3.1. Instead, both LG at tree-level and TG at loop-level are included on the same footing. Finally, class 8 contains four-fermion operators. They can contribute to the process through, for example, the penguin diagrams topologies shown in Fig. 5.2

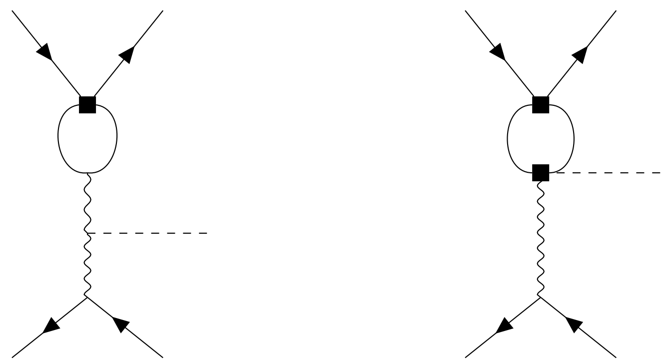

Figure 5.2: Penguin diagrams topologies contributing to the NLO VBF process.

Only the first topology is studied, since the others contains two NP vertices. The fermionic loop can contain leptons or quarks, as shown in Figure 5.3.

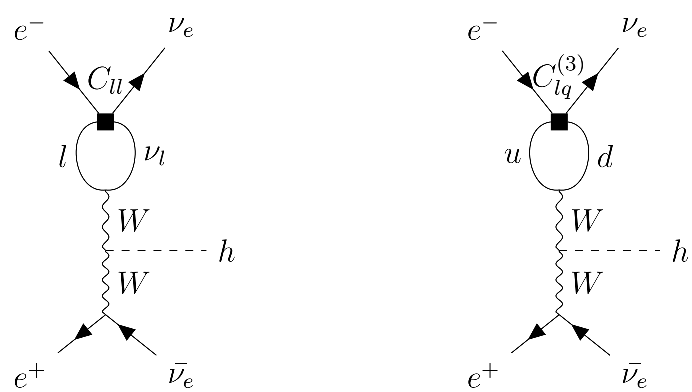

Figure 5.3: 4-fermion operators contributing to the penguin diagrams.

The only SMEFT operator that contributes to the 4-lepton vertex in the left diagram of Figure 5.3 is $\mathcal{O}_{ll}$. Indeed, $\mathcal{O}_{le}$ does not contribute because only left-handed fermions can couple to the W boson.

In the case of a quark loop, as in the diagram on the right of Figure 5.3, the only SMEFT contribution comes from $\mathcal{O}_{lq}^{(3)}$. Indeed, the operator $\mathcal{O}_{lq}^{(1)}$ does not enter because its isospin structure does not mix neutrinos and electrons. This is instead possible for $\mathcal{O}_{lq}^{(3)}$ due to the presence of the Pauli matrices in the current.

The number of independent WCs associated to these operators, under the MFV assumption, is studied in 3.1.

5.1 UV Renormalization

5.1.1 Renormalization of EFTs

When a theory is studied at NLO, i.e. one-loop corrections are added to the tree-level (TL) process, UV divergencies arise from loop computations. The bare Lagrangian is rewritten as the sum of a

renormalized Lagrangian containing finite and physical parameters and a counterterm Lagrangian. The coefficient of the latter are chosen such that they cancel the divergencies stemming from the bare Lagrangian order by order in perturbation theory. This is necessary to get finite physical predictions. Renormalizable theories, such as the SM, require only a finite number of counterterms to absorb all the divergent contributions. Indeed, the SM is described by a finite number of input parameters, whose values are fixed by experiments. Each physical quantity can be expressed as a function of these input parameters. As a consequence, an infinite number of predictions follow from a finite number of measurements and, therefore, from a finite number of counterterms.
An infinite number of counterterms is instead needed to cancel all the divergences for non-renormalizable theories since the number of free parameters is not finite. This is the case for EFTs, for example the SMEFT. Nevertheless, the latter is renormalizable order by order in the EFT expansion.
A generic EFT Lagrangian can be written as

$$\mathcal{L}_{\text{EFT}} = \sum_{\mathcal{D}>0} \sum_{i} \frac{c_i^{(\mathcal{D})} \mathcal{O}_i^{(\mathcal{D})}}{\Lambda^{\mathcal{D}-d}}, \tag{5.1}$$

where i is an index running over all the different $\mathcal{D}$ mass dimension operators.
In the previous expression, we denote the dimension of space-time with d. Multiple insertions of operators with $\mathcal{D} > d$ can generate operators of arbitrarily high dimension. For example, in order to remove divergences stemming from a 1-loop process with two insertions of a dimension-5 operator, a dimension-6 counterterm is needed, as showed in Figure 5.4.

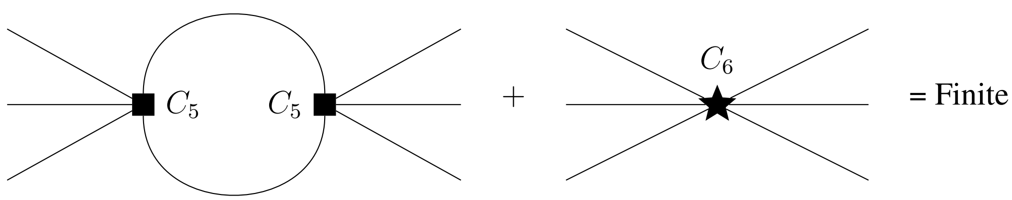

Figure 5.4: Dimension-6 counterterm needed to cancel the divergencies stemming from the 1-loop amplitude with two insertions of a dimension-5 operator.

This means that the Lagrangian contains a new dimension-6 operator with a WC $c_6(\mu)$ evolving with the energy scale μ through its Renormalization Group Equation (RGE) that contains a term proportional to the second power of the dimension-5 WC. Multiple insertions of the new dimension-6 operators would need a dimension-8 counterterm to cancel divergencies stemming from 1-loop processes and so on. Hence, non-renormalizable theories are those with operators of dimension $\mathcal{D} > d$ because an infinite number of counterterms is needed to renormalize the theory.
Conversely, renormalizable terms are only those with mass dimension $\mathcal{D} \leq d$. A theory is referred to as "renormalizable" if this condition holds for all its operators.
Nevertheless, if we consider a fixed expansion order, then only a finite number of counterterms is needed to renormalize all the divergences [20]. We work at dimension-six, hence only the renormalization constants for such operators are required to renormalize the theory. Practically, this corresponds to neglecting diagrams having multiple insertions of dimension-6 operators.

5.1.2 Electroweak input schemes in the SMEFT

SMEFT predictions depend on the input parameters and the renormalization schemes in which they are defined. In the EW sector of the SM, 3 input parameters are needed. There are different schemes for such input, depending on which observables are measured with the best accuracy. Indeed, it would be desireable to not have large uncertainties, otherwise they would propagate into all predictions. Moreover, input parameters introduce a number of WCs into physical observables, as, in the SMEFT, they can receive corrections from dimension-6 operators. It is preferred to keep this number small, so that the predictions mainly depend on dimension-6 operators describing new interactions for that specific process rather than on those entering as NLO corrections to the input parameters.

Predictions given with two different schemes are the same only if loop corrections are computed to all orders. However, one can make computations only at finite orders. An input scheme can indeed make the perturbative expansion converge faster than another one. The input scheme we use is the α_μ scheme, whose EW input parameters are the masses of the heavy vector bosons M_Z and M_W and the Fermi constant G_F. This is the preferred scheme in SMEFT because it reduces the dependence on WCs in propagators, as it includes both the weak gauge boson masses [21]. In addition, all the WCs of the SMEFT operators contributing to the process, already listed in Sect. 5, are renormalized in the $\overline{\text{MS}}$ scheme, which means that their counterterms are chosen to subtract the UV-divergent poles together with the universal finite term $\ln(4\pi) - \gamma_E$, where γ_E is the Euler-Mascheroni constant. We use a hybrid scheme for the renormalization of our parameters, i.e. masses and coupling are defined using different schemes. The masses of the heavy vector bosons are defined in the On-Shell (OS) scheme. This means that the finite parts of their counterterms are fixed such that the renormalized masses are equal to the poles of their respective propagators. Finally, the Fermi constant G_F is measured in muon decay. Historically, it is defined as a WC of the 4-fermion operator in the Fermi effective theory. It is calculated in [22], by matching the SMEFT onto this effective theory, by integrating out the W, Z, h bosons and the top quark from the SMEFT Lagrangian. The quantity that we actually renormalize is the VEV v of the Higgs field, which is related to G_F through the renormalization condition of the α_μ scheme:

$$v = \left(\frac{1}{\sqrt{2}G_F}\right)^{1/2} \tag{5.2}$$

This relation must hold at all orders in perturbation theory.

5.1.3 Tadpole renormalization

S-matrix elements are made finite by only renormalizing the input parameters and the fields of the theory, without introducing tadpoles at all. Tadpoles are diagrams where a single field is connected to a loop without further external legs. We cannot have tadpoles of the charged fields $W^\pm$ or $G^\pm$, as the vacuum is neutral. Those diagrams, therefore, would violate charge conservation. We do not have tadpoles of vector fields Z^μ or A^μ either, as the vacuum is invariant under Lorentz transformation. Hence, a vector with a VEV different from zero would violate Lorentz symmetry. Finally, also tadpoles of G^0 are not present, as it is a CP-odd pseudoscalar, whereas the vacuum is CP-even. Therefore, the only non-vanishing tadpole diagrams are those involving the physical

Higgs field. These tadpoles represent quantum corrections that generate terms linear in the physical Higgs field h when the potential of the Higgs doublet in eq. (2.17) is expanded around its Vacuum Expectation Value (VEV).
In R_ξ-gauge, an additional renormalization constant for the VEV of the Higgs field is necessary if one wants to render all n-point Green's functions finite. Nevertheless, parameters, like masses, can still depend on the gauge.
The tadpole diagrams T_h which carry an explicit dependence on the gauge-fixing parameter ξ are those with a Goldstone boson running in the loop, as in Fig. 5.5. Hence, in unitary gauge, we do not have a gauge dependence since Goldstone bosons are not present.

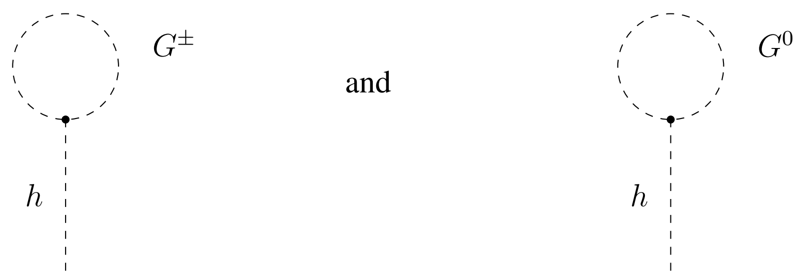

Figure 5.5: Gauge-dependent diagrams of T_h.

In the conventional scheme, where only 1PI diagrams are consider at NLO, hence no tadpoles are included, parameter definitions can be gauge-dependent.
Conversely, the Fleischer-Jegerlehner (FJ) tadpole scheme [8, 23] is used to have gauge-independent physical parameters. In this case, tadpole contributions are added to the 1PI diagrams, as explained in detail in the following to define a gauge-independent heavy vector boson mass.
The implementation of the FJ scheme consists in redefining the bare Higgs VEV v_0 such that the expansion of the Higgs field is performed around the minimum of the loop-corrected Higgs potential, rather than the tree-level one. This translates into the following equation:

$$v_0 = v_0^{\text{FJ}} + \Delta_v, \qquad \text{where} \quad \Delta_v = \frac{T_h}{m_h^2}. \tag{5.3}$$

v_0^{FJ} is the shifted VEV and it is renormalized as

$$v_0^{\text{FJ}} = v^{\text{FJ}} + \delta v^{\text{FJ}} \tag{5.4}$$

where the counterterm δv^{FJ} is gauge independent.
Inserting eq. (5.4) into eq. (5.3) and defining a counterterm δv for v_0,

$$v_0 = v^{\text{FJ}} + \delta v^{\text{FJ}} + \Delta_v = v^{\text{FJ}} + \delta v \tag{5.5}$$

one finds how the new gauge-independent counterterm is related to the latter:

$$\delta v^{\text{FJ}} = \delta v - \Delta_v. \tag{5.6}$$

Performing this shift everywhere in the Lagrangian is equivalent to introduce the tadpole contributions, in addiction to the One-Particle Irreducible (1PI) diagrams, at NLO. We illustrate this

point with the example of the vector boson masses counterterm in the FJ scheme, needed in the renormalization of our process.
In the conventional scheme, the UV-divergent terms of the 1PI corrections to the vector boson propagator are canceled by the counterterm, represented with a star in Figure 5.6.

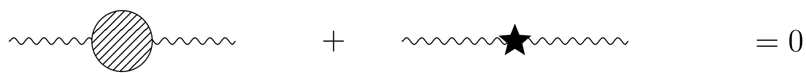

Figure 5.6: Definition of the vector boson squared mass counterterm in the conventional scheme. This counterterm, represented by the starred propagator, is gauge-dependent. This equation holds for the divergent part.

From eq. (5.6) and being the masses of the vector bosons proportional to the Higgs VEV, it follows that the counterterm of the vector boson squared mass is

$$\delta m_V^{2\,\mathrm{FJ}} = \delta m_V^2 - 2\Delta_v. \tag{5.7}$$

There are two equivalent ways to obtain the gauge-independent quantity $\delta m_V^{2\,\mathrm{FJ}}$.
We can shift the VEV to its correct minimum of the Higgs loop-corrected scalar potential everywhere in the Lagrangian without adding regular tadpoles in the NLO diagrams. They are indeed canceled by the counterterms for the 1-point function of the Higgs field, as shown in Figure 5.7.

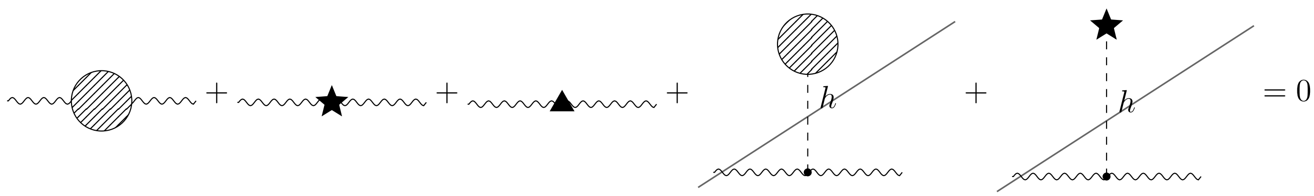

Figure 5.7: Diagrams to be added to the mass squared counterterm in order to remove the UV divergences and get a gauge-independent result. The shift of the vev, represented by the triangle insertion, is implemented. Regular tadpoles do not enter as they are removed by the counterterm for the 1-point function of the Higgs field.

The triangle in Figure 5.7 represents a counterterm insertion due to the VEV shift.
A second implementation method consists of adding the Higgs tadpoles to the 1PI diagrams. In this second case, the UV-divergent contributions stemming from the insertion due to the VEV shift are canceled by the counterterms for the 1-point function of the Higgs field, as shown in Figure 5.8.

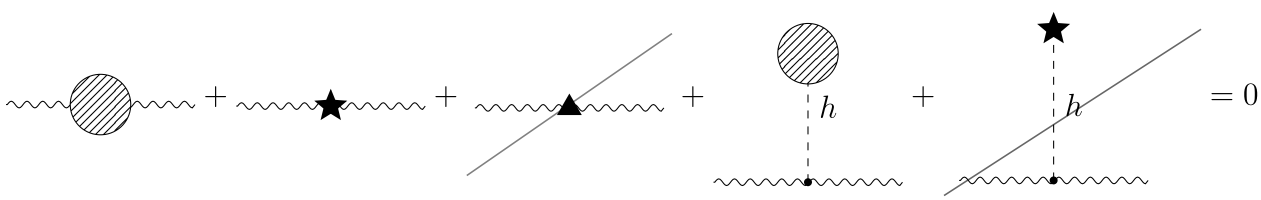

Figure 5.8: Diagrams to be added to the mass squared counterterm in order to remove the UV divergences and get a gauge-independent result. Regular tadpoles are added to the 1PI diagrams. The VEV shift, represented by the triangle insertion, does not enter as it cancels with the counterterms for the 1-point function of the Higgs field.

From a practical point of view, this means that one considers also the diagrams containing tadpoles, whereas the first method treats them as a counterterm in the propagator of all the particles which couple to the Higgs boson. This second method is the one we exploited for the VBF renormalization. From a diagrammatic perspective, the gauge-independent FJ counterterm for a massive vector boson can be represented as in Figure 5.9 when the VEV in shifted or as in Figure 5.10 when the regular tadpole contributions are added, as in our case.

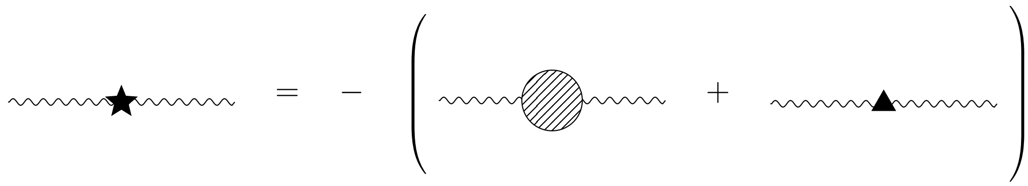

Figure 5.9: Diagrammatic representation of the gauge-independent counterterm for the squared vector boson mass when the VEV shift is performed.

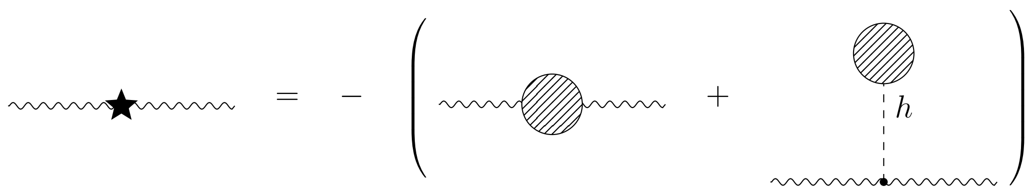

Figure 5.10: Diagrammatic representation of the gauge-independent counterterm for the squared vector boson mass when the 1-loop tadpoles are added to the 1PI diagrams.

5.2 IR divergences

After the UV renormalization of the theory, the VBF NLO amplitude contains IR divergences. In Dimensional Regularization (DR), where we work in a $d = 4 - 2\epsilon$ dimensional space-time, they manifest themselves through single and double poles in $1/\epsilon$. In order to remove the IR divergences arising from the virtual contributions, real photon emission contributions from the initial charged states must be included.

IR divergences are classified as soft or collinear. We have a virtual soft IR divergence when the momentum of a photon inside a loop integral goes to zero. They are canceled by real soft IR divergences. The latter accour because a detector with energy resolution ΔE is not able to distinguish a state with a single electron $|e^- >$ from the state $|e^- + \gamma_{\text{soft}} >$, where the electron emits a photon with an energy lower than the detector resolution. Hence, from an experimental point of view, these two states are degenerate. The consequence of this experimental limit to the accuracy with which energy states can be measured is that some energy will always be lost in emitted soft photons. What one actually observes is the sum of the elastic process, in which no photons are emitted, and the one in which some energy, up to the detector resolution, is lost in photons.

The tree level cross-section process involving a single emitted photon is of the same order, in the electromagnetic coupling, as a 1-loop correction to the original process with no emitted radiation. The cancellation of soft IR divergences between the NLO elastic process, where photons only

appear in virtual corrections, and the inelastic process, with energy loss from real photon emissions less that ΔE, persists to all orders in perturbation theory [24].
Collinear virtual divergences appear in one-loop diagrams when a photon inside a loop is parallel to an external massless particle. Accordingly, collinear real divergences are present when a massless fermion emits a photon with momentum parallel to its own. When the energy of this photon goes to zero, both soft and collinear divergences are present and they correspond to double poles in $1/\epsilon$ in the virtual corrections.
There are different IR subtraction schemes one can implement to cancel the soft divergences. `Whizard`, which we employ for our Montecarlo implementation of the phase space integrals, uses the FKS subtraction scheme, explained in detail in Appendix A.
After exploiting the FKS subtraction scheme, the amplitude is still divergent as it contains single poles in $1/\epsilon$ due to the collinear initial state divergences. Indeed, real initial state collinear divergences do not cancel automatically with those from virtual diagrams. In order to have a finite amplitude one can exploit the massification procedure [3], which consists of restoring the leading logarithmic dependence of the amplitude on the electron mass. From a practical point of view, this means that collinear single poles in $1/\epsilon$ are substituted by

$$\frac{1}{\epsilon} \to \log\left(\frac{s}{m_e^2}\right), \tag{5.8}$$

where s is the Mandelstam variable $s = (q_1 + q_2)^2$ with q_1 and q_2 the momenta of the initial state particles. In the limit of massless electron $m_e \to 0$ we recover the collinear IR divergences.

Chapter 6

Comparison of the numerical and analytical UV pole

In this chapter, we build the framework to renormalize the VBF within the SM. We analitically compute the UV pole in $1/\epsilon$ of the counterterm amplitude with `FeynArts` and `FeynCalc` [25–29]. This must be the opposite of the pole we get from `GoSam`, in order to cancel the UV divergences stemming from the NLO amplitude.
The output of `GoSam` is the term proportional to $1/\epsilon$ of the interference between the Tree Level (M_{TL}) and the Counterterm (M_{CT}) amplitude, normalized to the Born (M_{B}):

$$\frac{1}{4} \cdot 2\,\text{Re} \sum_{\text{Pol.}} (M^*_{\text{TL}} M_{\text{CT}}). \tag{6.1}$$

The Born amplitude is

$$M_{\text{B}} = \frac{1}{4} \sum_{\text{Pol.}} |M_{\text{TL}}|^2 = \frac{1}{4} M_{\text{TL}}{}^* M_{\text{TL}}, \tag{6.2}$$

The factor of $1/4$, both in eq. (6.1) and eq. (6.2) is the spin average factor.

6.1 Counterterm amplitude

The TL amplitude is:

$$iM_{\text{TL}} = iA\Big(\bar{u}(p_1)\gamma_\mu P_L u(q_1)\Big) \frac{-ig^{\mu\rho}}{(p_2 - q_2)^2 - M_W^2} g_{\rho\sigma} \frac{-ig^{\sigma\nu}}{(p_3 + p_2 - q_2)^2 - M_W^2} \Big(\bar{v}(q_2)\gamma_\nu P_L v(p2)\Big), \tag{6.3}$$

where

$$A = \frac{4}{v^3} M_W^4.$$

The notation used for the momenta is shown in Figure 6.1.

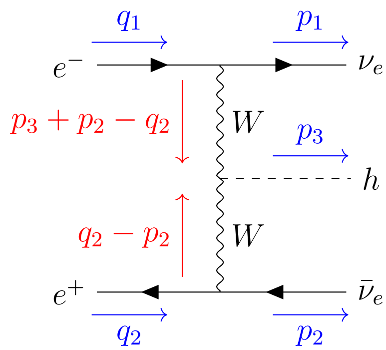

Figure 6.1: Convention of momenta for the VBF Feynman diagram.

The Feynman rules used to compute M_{TL} are:

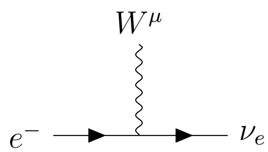

$$= -i\sqrt{2}\frac{M_W}{v}\gamma^\mu P_L$$

and

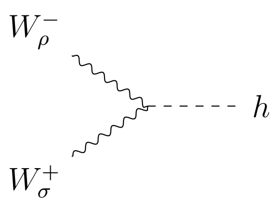

$$= 2i\,\frac{M_W^2}{v}\,g^{\rho\sigma}.$$

M_{CT} depends on the counterterms of the input parameters and on the wavefunction renormalization constants of the external fields. The only input parameters in M_{TL} are M_W and $G_F = 1/(\sqrt{2}\,v^2)$. Hence, M_{CT} can be written as:

$$M_{\text{CT}} = \frac{\partial M_{\text{TL}}}{\partial M_W}\delta M_W + \frac{\partial M_{\text{TL}}}{\partial(1/v^2)}\delta(1/v^2) + M_{\text{TL}} \cdot Z_e Z_{\nu_e}\sqrt{Z_h}, \tag{6.4}$$

where δM_W is the counterterm of the W mass, $\delta(1/v^2)$ the counterterm associated to the quantity $1/v^2$ (following the definitions given in [22]), Z_e, Z_{ν_e} and Z_h the wavefunction renormalization constants of the electron, the neutrino and the Higgs boson field, respectively. The wavefunction renormalization constant associated to the field f can be written as

$$Z_f = 1 + \delta Z_f, \tag{6.5}$$

where δZ_f contains the UV divergent term in $1/\epsilon$. Hence, the relevant part of the Lagrangian can be expanded as

$$M_{\text{CT}} \supset M_{\text{TL}}\left(\delta Z_e + \delta Z_{\nu_e} + \frac{1}{2}\delta Z_h\right). \tag{6.6}$$

We have validated the expression in Eq. (6.4) by an analytic computation of UV divergent parts at one-loop order obtained with the same computational framework.

In the next sections, we detail how the counterterms are determined, focusing on the divergent part. The masses of all the charged fermions contributing to the self-energy diagrams have been kept different from zero. This is only a computational expedient to avoid that IR divergencies are mixed with purely UV divergences. Nevertheless, since we are studying the VBF at very high energies, all the fermions but the top are taken to be massless after the pole extraction.

6.1.1 UV pole of the M_W counterterm

The UV pole of the counterterm for M_W has been computed by imposing that the UV divergences of the 1-loop corrections of the W boson propagator are canceled by the counterterm insertion

$$\delta\Gamma^W_{\mu\nu}(k) = -\delta Z_W(k^2 g_{\mu\nu} - k_\mu k_\nu) + (\delta M_W^2 + M_W^2 \delta Z_W) g_{\mu\nu}. \tag{6.7}$$

The one-loop UV-divergent self-energy can be expressed as

$$\Sigma^W_{\mu\nu}(k) = A(k^2 g_{\mu\nu} - k_\mu k_\nu) + B\ M_W^2 g_{\mu\nu}. \tag{6.8}$$

In $\Sigma_{\mu\nu}$ we do not only include 1PI diagrams but also the Higgs tadpoles in order to implement the FJ scheme, as explained in detail in Sect. 5.1.3.
The counterterm insertion must satisfy:

$$\left(\delta\Gamma^W_{\mu\nu}(k) + \Sigma^W_{\mu\nu}(k)\right)_{\text{div}} = 0, \tag{6.9}$$

diagrammatically represented in Figure 6.2.

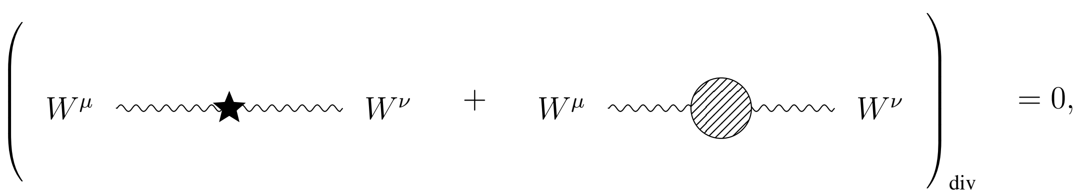

Figure 6.2: Diagrammatic representation of the renormalization condition in eq. (6.9).

where the subscript div stresses that this only holds for the divergent part. Equation (6.9) does not put any condition on the finite parts of the counterterm. However, at the present stage, we are interested in the divergent parts only, hence it is not necessary to provide a prescription for the finite terms.
Equations (6.8,6.9) provide $A - \delta Z_W{}^{\text{div}} = 0$ which immediately gives $\delta Z_W{}^{\text{div}} = A$. This means that A can be extracted by selecting the coefficient of k^2 from the one-loop self-energy $\Sigma^W_{\mu\nu}(k)$.
Subsequently, one determines the counterterm for the squared W mass δM_W^2 by imposing

$$B\ M_W^2 = \delta M_W^2 + M_W^2 \delta Z_W \quad \to \delta M_W^2 = M_W^2(B - A). \tag{6.10}$$

Finally, δM_W is given by:

$$\delta M_W = \frac{1}{2M_W} \delta M_W^2. \tag{6.11}$$

The analytic expression of δM_W can be found in the Appendix B.

6.1.2 UV pole of the wavefunction renormalization constants

We now discuss how we compute the leptonic renormalization constants. There is no difference between the electron and the muon wavefunction renormalization constants in the limit of massless fermions and flavour conservation, as well as for the renormalization constants of the two neutrinos. The self energy $\Sigma^f(p)$ of a massless fermion f can be decomposed as [30]

$$\Sigma^f(p) = \not{p} P_L \Sigma^f_L(p^2) + \not{p} P_R \Sigma^f_R(p^2). \tag{6.12}$$

The UV pole of the wavefunction renormalization constant of the left-handed fermion is the same but opposite sign of the divergent part of $\Sigma^f_L(p^2)$. Only the left-handed counterterm is needed, as it follows from the chiral structure of Eq. (6.3).
First of all, we compute the 1-loop self energy of the fermion f

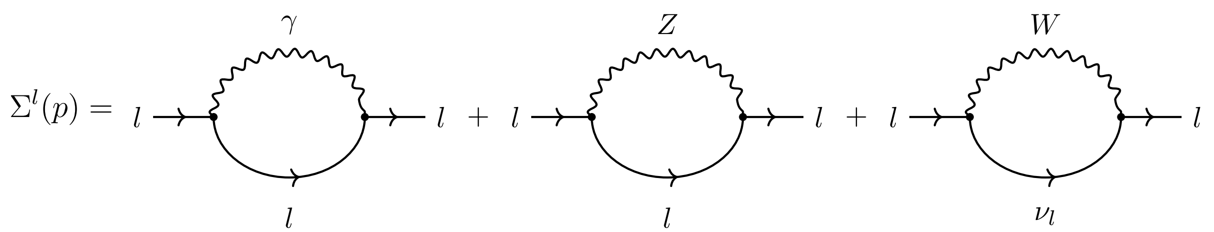

if f is a charged lepton and

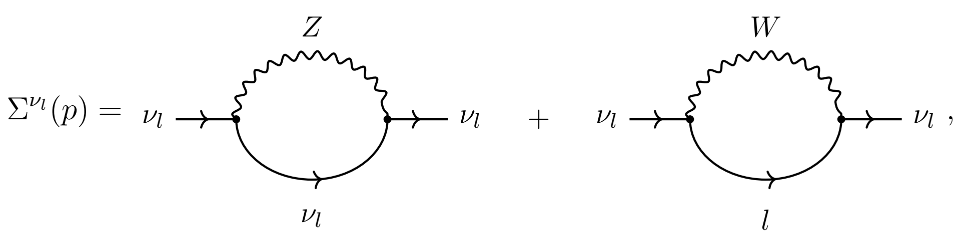

if f is a neutrino. In the latter case there is no correction involving the photon, as neutrinos are chargeless.
From eq. (6.13) we have

$$\begin{aligned}
&\mathrm{tr}[\Sigma^f(p)\not{p}P_R] = \\
=&\Sigma^f_L(p^2)\frac{p_\mu p_\nu}{4}\mathrm{tr}[\gamma^\mu(1-\gamma_5)\gamma^\nu(1+\gamma_5)] + \Sigma^f_R(p^2)\frac{p_\mu p_\nu}{4}\mathrm{tr}[\gamma^\mu(1+\gamma_5)\gamma^\nu(1+\gamma_5)] = \\
=&\Sigma^f_L\frac{p_\mu p_\nu}{4}2\underbrace{\mathrm{tr}[\gamma^\mu\gamma^\nu]}_{4g^{\mu\nu}} = \\
=&2p^2\Sigma^f_L(p^2),
\end{aligned} \tag{6.13}$$

so we can obtain the wavefunctions renormalization constants as

$$\delta Z_f = -\Sigma^f_L(p^2) = -\frac{\mathrm{tr}[\Sigma^f(p)\not{p}P_R]}{2p^2}. \tag{6.14}$$

The analytic expressions for δZ_l and δZ_{ν_l} can be found in Appendix B.

The UV pole of the h wavefunction renormalization constant has been computed by imposing that the UV divergences of the 1-loop corrections of the h boson propagator are canceled by the counterterm insertion

$$\delta\Gamma^h(k^2) = -k^2\delta Z_h + (\delta M_h^2 + M_h^2\delta Z_h). \tag{6.15}$$

The one-loop UV-divergent self-energy can be expressed as

$$\Sigma^h(k^2) = Ak^2 + B. \tag{6.16}$$

In this case we do not need to include the contribution of the Higgs tadpoles in $\Sigma^h(k^2)$. Indeed, the wavefunction renormalization is determined by the term of the self energy depending on the momentum of the particle flowing through the 2-point function. Loop tadpole integrals are just constants, namely they are momentum-independent and therefore they do not contribute to δZ_h. Tadpoles can only renormalize masses or the VEV.
The counterterm insertion must satisfy

$$\left(\delta\Gamma^h(k^2) + \Sigma^h(k^2)\right)_{\text{div}} = 0, \tag{6.17}$$

that can diagrammatically be represented as in Figure 6.17.

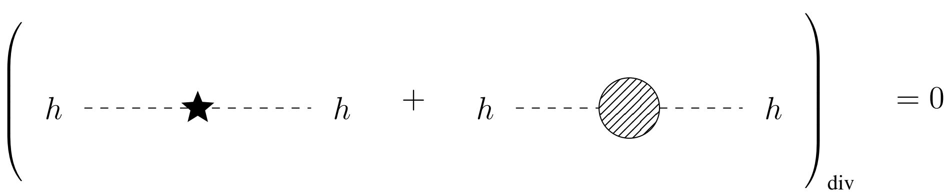

Figure 6.3: Diagrammatic representation of eq. (6.17).

In order to find the UV term of the h wavefunction constant, one can impose $A - \delta Z_h^{\text{div}} = 0$ which immediately gives $\delta Z_h^{\text{div}} = A$. As in Sect. 6.1.1, A can be extracted by selecting the coefficient of k^2 from the one-loop self-energy $\Sigma^h(k^2)$. The analytic expression for δZ_h^{div} can be found in the Appendix B.

6.1.3 UV pole of the VEV counterterm

The NLO muon decay can be describe by the following effective Lagrangian:

$$\mathcal{L}_{\text{eff}} = \mathcal{L}_{\text{QED}} + \mathcal{L}_{\text{F}}, \tag{6.18}$$

where the Lagrangian of quantum electrodynamics reads

$$\mathcal{L}_{\text{QED}} = -\frac{1}{4}F_{\mu\nu}F^{\mu\nu} + \bar{\Psi}(i\gamma^\mu D_\mu - m)\Psi, \quad \Psi = e, \mu \tag{6.19}$$

and the Fermi Lagrangian $\mathcal{L}_{\text{F}}$ is instead

$$\mathcal{L}_{\text{F}} = -2\sqrt{2}\, G_F(\bar{\nu}_\mu\gamma_\nu P_L\mu)(\bar{e}\gamma^\nu P_L\nu_e). \tag{6.20}$$

The Fermi constant is calculated by matching the effective Lagrangian $\mathcal{L}_{\text{eff}}$ with $\mathcal{L}_{\text{SM}}$ from which the heavy electroweak bosons W, Z, H and the top quark have been integrated out.
The VEV of the Higgs field is defined as a function of G_F through the renormalization condition in eq. (5.2).
Following the notation in [22], the bare VEV v_0 and the renormalized one v are related through eq. (6.21)

$$\frac{1}{v_0^2} = \frac{1}{v^2} + \delta\left(\frac{1}{v^2}\right) = \frac{1}{v^2}\left(1 - \frac{1}{v^2}\Delta v^{(4,1,\mu)}\right), \tag{6.21}$$

where the superscript $(4,1,\mu)$ symbolizes that we are working with SM 4-dimensional operators, at 1 loop order and in the α_μ scheme, respectively.
Using the same notation as in eq. (6.21), the bare SM amplitude for the muon decay can be written as

$$A_0^{\text{SM}} = -\frac{2}{v_0^2}\left(A_0^{(4,0)} + \frac{1}{v_0^2}A_0^{(4,1)}\right)S_\mu, \tag{6.22}$$

where

$$S_\mu = \Big(\bar{u}(q_2)\gamma_\nu P_L v(q_3)\Big)\Big(\bar{u}(q_1)\gamma^\nu P_L u(p)\Big). \tag{6.23}$$

The momenta of the spinors in eq. (6.23) are understood from Figure 6.4.

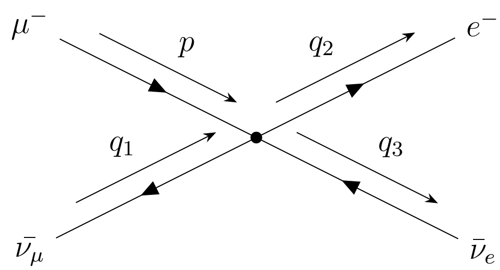

Figure 6.4: Feynman diagram for the 4-fermion interaction in the muon decay.

$A_0^{(4,0)}$ and $A_0^{(4,1)}$ are SM coefficient of the amplitude at TL and at NLO, respectively.
The effective amplitude reads, instead,

$$A^{\text{eff}} = -\frac{2}{v^2}S_\mu. \tag{6.24}$$

Following [22], the matching is perfomed off-shell, where all the masses and external momenta are set to 0. Hence, loop corrections involve only photons and yield scaleless integrals, which can be set to 0. The counterterm of the VEV is calculated by ensuring the condition in eq. (5.2) in the α_μ scheme. This translates into the requirement that the renormalized SM amplitude matches order by order in perturbation theory to A^{eff}:

$$A^{\text{SM}} = -\frac{2}{v^2}\left(A^{(4,0,\mu)} + \frac{1}{v^2}A^{(4,1,\mu)}\right)S_\mu \stackrel{!}{=} A^{\text{eff}}. \tag{6.25}$$

The renormalization condition in eq. (6.25) can be applied to eq. (6.22), once the bare VEV has been substituted by eq. (6.21) and the external fields have been written as the renormalized ones multiplied by the square root of their wavefunction renormalization constants:

$$-\frac{2}{v^2}\left(1-\frac{1}{v^2}\Delta v^{(4,1,\mu)}\right)\left(A^{(4,0,\mu)}+\frac{1}{v^2}A^{(4,1,\mu)}\right)S_\mu\left(1+\frac{1}{2}\Delta Z_f\right)\stackrel{!}{=}-\frac{2}{v^2}S_\mu, \tag{6.26}$$

where

$$\Delta Z_f=\Delta Z_\mu+\Delta Z_{\nu_\mu}+\Delta Z_e+\Delta Z_{\bar{\nu}_e}. \tag{6.27}$$

Notice that ΔZ_f contains only the contribution from the W and the Z, since the photon corrections vanish because they are scaleless.
In eq. (6.27), the square root of the wavefunction renormalization constant of a generic lepton l has been Taylor expanded as

$$\sqrt{Z_l}=\sqrt{1+\Delta Z_l}\simeq 1+\frac{1}{2}\Delta Z_l. \tag{6.28}$$

Collecting terms order by order in perturbation theory as in eq. (6.29)

$$\underbrace{-\frac{2}{v^2}A^{(4,0,\mu)}S_\mu}_{\text{TL}}\underbrace{-\frac{2}{v^4}\left(A^{(4,1,\mu)}-\Delta v^{(4,1,\mu)}+\frac{1}{2}\Delta Z_f\,v^2\right)S_\mu}_{\text{NLO}}+\ldots\stackrel{!}{=}-\frac{2}{v^2}S_\mu, \tag{6.29}$$

the following relations yield:

$$\begin{cases}A^{(4,0,\mu)}=1\\ A^{(4,1,\mu)}-\Delta v^{(4,1,\mu)}A^{(4,0,\mu)}+\frac{1}{2}A^{(4,0,\mu)}\Delta Z_f\,v^2=0\end{cases} \tag{6.30}$$

From eq. (6.30), one finally finds the expression of the VEV counterterm in the SM using the α_μ renormalization scheme:

$$\delta\left(\frac{1}{v^2}\right)=-\frac{1}{v^4}\Delta v^{(4,1,\mu)}=-\frac{1}{v^4}\left(A^{(4,1,\mu)}+\frac{1}{2}\Delta Z_f\right). \tag{6.31}$$

The wavefunction renormalization constants in ΔZ_f are calculated as detailed in subsection 6.1.2. $A^{(4,1,\mu)}$ is instead calculated as

$$A^{(4,1,\mu)}=-\frac{A^{\mu\text{ decay}}_{\text{NLO}}}{(2/v^4)}, \tag{6.32}$$

where $A^{\mu\text{ decay}}_{\text{NLO}}$ is the NLO amplitude of the muon decay in the SM. As discussed before, the FJ tadpole scheme has been applied, so tadpole diagrams have been included in the computation. The analytic expression of $\delta(1/v^2)$ can be found in Appendix B. We have compared our final result with [22]. We stress that this reference performs the computation in the unitary gauge, but since in our tadpole scheme δv is gauge independent, a comparison of this intermediate result can be performed. We mention, however, that the tadpole contribution and the 1PI contribution are, individually, gauge dependent, whereas their sum is gauge-independent.

6.2 Numerical comparison of the UV pole

The numerical quantity we want to compare with GoSam is the UV pole of

$$\frac{2\,\mathrm{Re}(M^*_{\mathrm{TL}}M_{\mathrm{CT}})}{M_B}. \tag{6.33}$$

The analytical expression of eq. (6.33), obtained using the Mathematica package FeynCalc is:

$$\begin{aligned}&\frac{256\,M_W^7\,(\bar{p}_1\cdot\bar{q}_2)\,(\bar{p}_2\cdot\bar{q}_1)}{v^6\,\Delta_1^3\,\Delta_2^3}\Bigg[\Big(\Delta_2-2M_W^2\Big)\Bigg(2(\bar{p}_2\cdot\bar{q}_2)\Big[8\,\delta M_W+3M_W\,\delta(1/v^2)\,v^2+2M_W\delta Z\Big]\\&+M_W^2\Big[4\,\delta M_W+3M_W\,\delta(1/v^2)\,v^2+2M_W\,\delta Z\Big]\Bigg)-4\,\delta M_W\,M_W^2\,\Delta_1\Bigg],\end{aligned} \tag{6.34}$$

where

$$\Delta_1=2(\bar{p}_2\cdot\bar{q}_2)+M_W^2,\qquad \Delta_2=-2(\bar{p}_2\cdot\bar{p}_3)+2(\bar{p}_2\cdot\bar{q}_2)+2(\bar{p}_3\cdot\bar{q}_2)-M_H^2+M_W^2 \tag{6.35}$$

and

$$\delta Z=\delta Z_e+\delta Z_{\nu_e}+\frac{1}{2}\delta Z_h. \tag{6.36}$$

GoSam gives the numerical result of the UV pole for a randomly chosen configuration of the external particle momenta. The values of the parameters are instead taken from a UFO model [31], created with SMEFTfr [32]. In this model the particle content, the parameters and the interaction vertices of the defined Lagrangian are described. We perform the computation within such framework, rather than relying on the GoSam SM built-in model file since the inclusion of the SMEFT operators, which represents the following stage of this study, will be straightforward.
In the following we compare the pole we get from eq. (6.34) with the numerical one from GoSam at $\sqrt{s}=350$GeV for different configurations for the momenta of the external particles:

momenta configuration	analytic pole	GoSam pole
1	0.016	-0.016
2	-0.128	0.122
3	-0.045	0.042

For the numerical evaluation, we used the following set of numerical parameters:
$M_W=80.4$GeV, $M_Z=91.2$GeV, $M_h=125$GeV, $G_F=1.16\cdot10^{-5}$GeV^{-2}, $M_t=173$GeV.
The three momenta configurations are:

Configuration 1:

$$q_1 = \begin{pmatrix} +175 \\ 0 \\ 0 \\ -175 \end{pmatrix}, \quad q_2 = \begin{pmatrix} +175 \\ 0 \\ 0 \\ +175 \end{pmatrix}, \quad p_1 = \begin{pmatrix} +119 \\ +101 \\ -18.9 \\ +60.0 \end{pmatrix}, \quad p_2 = \begin{pmatrix} +71.3 \\ -6.70 \\ -5.01 \\ -70.8 \end{pmatrix}, \quad p_3 = \begin{pmatrix} +159 \\ -94.8 \\ +23.9 \\ +10.8 \end{pmatrix}$$

Configuration 2:

$$q_1 = \begin{pmatrix} +175 \\ 0 \\ 0 \\ -175 \end{pmatrix}, \quad q_2 = \begin{pmatrix} +175 \\ 0 \\ 0 \\ +175 \end{pmatrix}, \quad p_1 = \begin{pmatrix} +81.1 \\ -3.08 \\ +57.2 \\ -57.4 \end{pmatrix}, \quad p_2 = \begin{pmatrix} +98.7 \\ -49.0 \\ +44.1 \\ +73.5 \end{pmatrix}, \quad p_3 = \begin{pmatrix} +170 \\ +52.0 \\ -101 \\ -16.1 \end{pmatrix}$$

Configuration 3:

$$q_1 = \begin{pmatrix} +175 \\ 0 \\ 0 \\ -175 \end{pmatrix}, \quad q_2 = \begin{pmatrix} +175 \\ 0 \\ 0 \\ +175 \end{pmatrix}, \quad p_1 = \begin{pmatrix} +147 \\ +111 \\ +87.1 \\ +39.2 \end{pmatrix}, \quad p_2 = \begin{pmatrix} +19.9 \\ -1.34 \\ -18.0 \\ -8.56 \end{pmatrix}, \quad p_3 = \begin{pmatrix} +183 \\ -110 \\ -69.2 \\ -30.6 \end{pmatrix}$$

Chapter 7

Conclusions and Outlook

In this thesis we analysed the production of a Higgs boson through Vector Boson Fusion (VBF) at a future e^+e^- collider. We introduced the SM of particle physics, presenting its main features and its limitations. Subsequently, we introduced the EFTs and, in particular, the SMEFT, as a possible parametrization to extend the SM by supplementing it with operators of higher dimension built with SM fields. We studied the truncation effects on the total cross section for $e^+e^- \to \nu_e\bar{\nu}_e h$ for one WC for each operator class of the Warsaw basis. We found that the quadratic contribution to the cross section in $1/\Lambda^2$ is negligible, as it contributes for less than 5% to the total result in the worst possible scenario, namely for $C_{\varphi W}$.
We then analyzed how to potentially disentangle the two different production channels, VBF and Higgsstrahlung (HS), for single Higgs production at lepton colliders. Practically, we analyzed how large could the interference between VBF and HS be at $\sqrt{s} = 350$ GeV at LO. We found that, for some combinations of the WCs, it can exceed 20% of either the VBF or the total cross section. Nevertheless, the interference progressively decreases with an increasing number of WC combinations, hence it has an important effect only for some WC combinations. Our findings allow us to focus on the VBF, as it is the dominant channel for the process $e^+e^- \to \nu_e\bar{\nu}_e h$ at the energy scale of interest.
We started the implementation of the NLO corrections to VBF, presenting the basis of SMEFT dimension-six operators which contribute. We described the α_μ input scheme and the FJ tadpole scheme in order to fix the theoretical framework for the UV renormalization. Furthermore, we discussed how to treat IR divergences.
Thus far, we extracted the UV pole in the SM, both analytically from the counterterm amplitude and from `GoSam`. We compared the two, validating our framework.
The goal of this project is the computation of the NLO EW corrections of the cross section for Higgs production via vector boson fusion at an e^+e^- collider in SMEFT. The SMEFT HS channel has already been widely studied and presented in the literature. Our goal would complete the SMEFT NLO analysis and would provide further information of the sensitivity on the considered operators in the high energy runs of future lepton colliders. Indeed, it would also be the missing piece to understand the interplay of other operators with the one modifying the trilinear Higgs self-coupling. In this way one could estimate the potential of the FCC-ee to measure the trilinear coupling. Moreover, this process can be used to study the off-shell Higgs decays into leptons and neutrinos, that would provide an additional missing ingredient for a complete SMEFT description at NLO. So far, indeed, an exhaustive picture of Higgs decays is missing. To conclude, a consistent

and complete NLO SMEFT study, including the single Higgs production in HS and VBF and the whole picture of Higgs decay, would allow us to fully exploit the potential of the FCC-ee in precision Higgs measurements and in capturing SMEFT effects.

Appendix A

The FKS subtraction scheme

The squared modulus of the UV renormalized amplitude at NLO accuracy for a given process can be written as

$$|M|^2 = |M_{\text{LO}}|^2 + 2\,\text{Re}(M_{\text{B}}^* M_{\text{V}}) + |M_{\text{R}}|^2 \tag{A.1}$$

where M_{LO} is the LO amplitude, M_{V} is the NLO virtual amplitude and M_{R} is the NLO real amplitude. Both the virtual and the real amplitudes diverge. The virtual IR divergences appear when a loop integral, with a photon flowing inside it, is computed. The virtual amplitude is integrating over the phase space for the n final particles involved in the process. The real cross section is instead computed by integrated $|M_{\text{R}}|^2$ over the phase space element for n+1 particles, as a photon is also present. This integral contains the IR poles.

`Whizard` integrates finite quantities at each phase space point. In order to obtain finite quantities, we need to remove the divergent terms of the real NLO amplitude, hence a subtraction scheme must be chosen. `Whizard` uses the FKS subtraction formalism, proposed by Frixione, Kunszt, and Signer [33]. For a generic $2 \to n$ scattering process, the real-emission contribution develops a large number of overlapping infrared (soft and collinear) singular regions as the number of external charged particles increases. The FKS subtraction scheme addresses this complexity by introducing a partition of the real-emission phase space into sectors through suitable partition functions. In each sector, only the soft and collinear singularities associated with a single FKS emitter are present, greatly simplifying the construction of the subtraction counterterms.

The FKS scheme classifies the IR divergences by defining a set $\mathcal{P}_{\text{FKS}}$ of ordered pairs of particles (i,j) that induce a soft singularity, a collinear one or both of them in the $n+1$ phase space. For the VBF process, this set can be defined as

$$\begin{aligned}\mathcal{P}_{\text{FKS}}(\text{VBF}) = \{(i,j) \;|\; & i=3,\; j=1,2,\\ & M_{\text{IR}} \to \infty \text{ if } k_i \to 0 \text{ or } \mathbf{k}_i \parallel \mathbf{k}_j\}\,,\end{aligned} \tag{A.2}$$

where $j=1,2$ corresponds to the initial state particles, the electron and the positron.

Using the notation $1 = e^-$, $2 = e^+$ and $3 = \gamma$, the pairs in $\mathcal{P}_{\text{FKS}}$ fot the VBF are:

- (3,1): γ is a soft photon and/or γ is emitted parallel to e^-
- (3,2): γ is a soft photon and/or γ is emitted parallel to e^+.

For each pair (i,j)$\in \mathcal{P}_{\text{FKS}}$, a positive-definite function S_{ij} is defined such that S_{ij} goes to zero in all regions of the phase space where M_{R} diverges, except if the i particle is soft or if i and j particles are collinear. The partition in the $n+1$ phase space can therefore be written as

$$M_{\text{R}} = \sum_{(i,j)\in\mathcal{P}_{FKS}} S_{ij} M_{\text{R}} \tag{A.3}$$

with

$$\sum_{(i,j)\in\mathcal{P}_{FKS}} S_{ij} = 1. \tag{A.4}$$

In each of these regions, the FKS subtraction scheme subtracts the local S term to the squared modulus of the real amplitude such that in an "unresolved limit", i.e. the limit in which M_{R} is divergent, the quantity $|M_{\text{R}}|^2 - S$ is finite. In order to restore the previous expression, the S term must also be added: this is performed by adding the integral of S over the phase space element of the photon, inside the integral over the n-particle phase space of the virtual contribution. The expression of the differential cross section for some observable O is therefore:

$$\frac{d\sigma}{dO} \sim \underbrace{\int d\Phi_n |M_{\text{LO}}|^2}_{\text{LO}} + \underbrace{\int d\Phi_n \left(2\,\text{Re}(M_{\text{B}}^* M_{\text{V}}) + \int d\Phi_1 S \right) + \int d\Phi_{n+1} (|M_{\text{R}}|^2 - S)}_{\text{NLO}}. \tag{A.5}$$

If the cross section was computed analytically, the virtual and real contributions would have the following structures:

$$\int d\Phi_n 2\,\text{Re}(M_{\text{B}}^* M_{\text{V}}) \sim \frac{A}{{\epsilon_{\text{IR}}}^2} + \frac{B'}{\epsilon_{\text{IR}}} + \frac{B''}{\epsilon_{\text{UV}}} + C \tag{A.6}$$

$$\int d\Phi_{n+1} |M_{\text{R}}|^2 \sim \frac{\tilde{A}}{{\epsilon_{\text{IR}}}^2} + \frac{\tilde{B}}{\epsilon_{\text{IR}}} + \tilde{C}, \tag{A.7}$$

where A, B', B'', C, $\tilde{A}$, $\tilde{B}$ and $\tilde{C}$ are real finite quantities.
The IR divergences from the virtual amplitude would have canceled the divergences stemming from the real amplitude if there had not been initial state collinear divergences (KLN theorem [34]). In other words, using the previous notation from the FKS formalism (A.2),

$$A = \tilde{A} \text{ and } B = \tilde{B} \text{ if } \mathbf{k}_i \nparallel \mathbf{k}_j, \quad (i,j) \in \mathcal{P}_{FKS}.$$

Once the FKS subtraction scheme has been applied, the virtual and the real soft IR divergences cancel each other out and the UV divergent terms of the virtual amplitude are canceled by the counterterms before the integration occurs: the expression of the cross section is therefore left with only the collinear initial state divergences.

Appendix B

Counterterms in the FJ scheme

The analytical expressions for the UV poles of the counterterms used to compute eq. (6.4) are presented below. They do not depend on the gauge choice, since the tadpole FJ scheme [8] has been implemented. Moreover, they do not depend on the fermion masses, as they have been set equal to zero, except the top mass.
The counterterm for the W boson mass is:

$$\begin{aligned}\delta M_W =&\frac{-M_W}{96 v^2 c_W^2 M_h^2 \pi^2 \epsilon}\Bigg(- 6\, C_W\, M_W\, M_Z^3 + 4\, C_W^4\, M_H^2\, (22\, M_W^2 + 3\, M_Z^2) \\ &+ C_W^2 \Big(9\, M_H^4 + 18\, M_H^2\, M_T^2 - 72\, M_T^4 - 92\, M_H^2\, M_W^2 + 36\, M_W^4 \\ &+ 3\, M_H^2\, M_Z^2 + 76\, M_H^2\, M_W^2\, S_W^2 \Big) + 12\, M_W^2\, (2\, M_Z^2 - M_H^2\, S_W^4) \Bigg),\end{aligned} \tag{B.1}$$

where S_W and C_W are the sine and cosine of the Weinberg angle, and they are defined as a function of the input parameters as:

$$C_W = \frac{M_W}{M_z}, \qquad S_W = \sqrt{1 - \frac{M_W^2}{M_Z^2}}. \tag{B.2}$$

The wave function renormalization constant for the lepton is

$$\delta Z_l = \frac{S_W^2}{16\pi^2 v^2 \epsilon} \frac{M_Z^4 - 4M_w^4 + 2M_W^2\, M_Z^2}{(M_W - M_Z)(M_W + M_Z)}, \tag{B.3}$$

the one for the neutrinos is

$$\delta Z_{\nu_l} = \frac{S_W^2 M_Z^2 (2M_W^2 + M_Z^2)}{16\pi^2 v^2 \epsilon (M_W - M_Z)(M_W + M_Z)}, \tag{B.4}$$

whereas the one for the Higgs boson reads:

$$\delta Z_h = \frac{M_W^2 - C_W^2 (3M_t^2 - 2M_W^2)}{8\pi^2 v^2 C_W^2 \epsilon}. \tag{B.5}$$

Finally, the counterterm associated with $1/v^2$ calculated from the muon decay and cross-checked with [22] yields:

$$\delta(1/v^2) = \frac{S_W^2 M_Z^2}{8\pi^2 v^4 \epsilon (M_W^2 - M_Z^2)^2} \cdot \Big(-3M_Z^2 S_W^2(-M_t^2 + 2M_W^2 + M_Z^2) - 2M_W^4 + M_W^2 M_Z^2 + M_Z^4 \Big). \tag{B.6}$$

Bibliography

[1] C. Degrande, G. Durieux, F. Maltoni, K. Mimasu, E. Vryonidou, and C. Zhang, "Automated one-loop computations in the standard model effective field theory," *Phys. Rev. D* **103** no. 9, (2021) 096024, `arXiv:2008.11743 [hep-ph]`.

[2] **FCC** Collaboration, A. Abada *et al.*, "Fcc physics opportunities: Future circular collider conceptual design report volume 1," *Eur. Phys. J. C* **79** (2019) 474, `arXiv:1811.10545 [hep-ex]`.

[3] K. Asteriadis, S. Dawson, P. P. Giardino, and R. Szafron, " $e^+e^- \to ZH$ process in the SMEFT beyond leading order," *JHEP* **02** (2025) 162, `arXiv:2409.11466 [hep-ph]`.

[4] A. Denner, S. Dittmaier, M. Roth, and M. M. Weber, "Electroweak radiative corrections to e+ e- —> nu anti-nu H," *Nucl. Phys. B* **660** (2003) 289–321, `arXiv:hep-ph/0302198`.

[5] G. Belanger, F. Boudjema, J. Fujimoto, T. Ishikawa, T. Kaneko, K. Kato, and Y. Shimizu, "Full one loop electroweak radiative corrections to single Higgs production in e+ e-," *Phys. Lett. B* **559** (2003) 252–262, `arXiv:hep-ph/0212261`.

[6] P. Bredt, T. Banno, M. Höfer, S. Iguro, W. Kilian, Y. Ma, J. Reuter, and H. Zhang, "Chasing the Two-Higgs-Doublet Model via Electroweak Corrections at e+e- Colliders," *Phys. Rev. Lett.* **136** no. 8, (2026) 081801, `arXiv:2509.05421 [hep-ph]`.

[7] J. Braun, B. Campillo Aveleira, G. Heinrich, M. Höfer, S. P. Jones, M. Kerner, J. Lang, and V. MagerySimpla, "One-loop calculations in effective field theories with GoSam-3.0," *SciPost Phys. Codeb.* **62** (2026) 1, `arXiv:2507.23549 [hep-ph]`.

[8] J. Fleischer and F. Jegerlehner, "Radiative Corrections to Higgs Decays in the Extended Weinberg-Salam Model," *Phys. Rev. D* **23** (1981) 2001–2026.

[9] C. C. Nishi, "Simple derivation of general Fierz-like identities," *Am. J. Phys.* **73** (2005) 1160–1163, `arXiv:hep-ph/0412245`.

[10] G. Isidori, F. Wilsch, and D. Wyler, "The standard model effective field theory at work," *Rev. Mod. Phys.* **96** no. 1, (2024) 015006, `arXiv:2303.16922 [hep-ph]`.

[11] C. Arzt, M. B. Einhorn, and J. Wudka, "Patterns of deviation from the standard model," *Nucl. Phys. B* **433** (1995) 41–66, `arXiv:hep-ph/9405214`.

[12] G. Buchalla, G. Heinrich, C. Müller-Salditt, and F. Pandler, "Loop counting matters in SMEFT," *SciPost Phys* **15** (2023) 088, `arXiv:2204.11808 [hep-ph]`.

[13] G. Guedes, P. Olgoso, and J. Santiago, "Towards the one loop IR/UV dictionary in the SMEFT: One loop generated operators from new scalars and fermions," *SciPost Phys.* **15** no. 4, (2023) 143, `arXiv:2303.16965 [hep-ph]`.

[14] D. A. Faroughy, G. Isidori, F. Wilsch, and K. Yamamoto, "Flavour symmetries in the SMEFT," *JHEP* **08** (2020) 166, `arXiv:2005.05366 [hep-ph]`.

[15] B. Grzadkowski, M. Iskrzynski, M. Misiak, and J. Rosiek, "Dimension-Six Terms in the Standard Model Lagrangian," *JHEP* **10** (2010) 085, `arXiv:1008.4884 [hep-ph]`.

[16] P. Azzurri, G. Bernardi, S. Braibant, D. d'Enterria, J. Eysermans, P. Janot, A. Li, and E. Perez, "A special Higgs challenge: measuring the mass and production cross section with ultimate precision at FCC-ee," *Eur. Phys. J. Plus* **137** no. 1, (2022) 23, `arXiv:2106.15438 [hep-ex]`.

[17] W. Kilian, T. Ohl, and J. Reuter, "WHIZARD: Simulating Multi-Particle Processes at LHC and ILC," *Eur. Phys. J. C* **71** (2011) 1742, `arXiv:0708.4233 [hep-ph]`.

[18] E. Celada, T. Giani, J. ter Hoeve, L. Mantani, J. Rojo, A. N. Rossia, M. O. A. Thomas, and E. Vryonidou, "Mapping the SMEFT at high-energy colliders: from LEP and the (HL-)LHC to the FCC-ee," *JHEP* **09** (2024) 091, `arXiv:2404.12809 [hep-ph]`.

[19] J. de Blas, A. Goncalves, V. Miralles, L. Reina, L. Silvestrini, and M. Valli, "Constraining new physics effective interactions via a global fit of electroweak, Drell-Yan, Higgs, top, and flavour observables," *JHEP* **03** (2026) 013, `arXiv:2507.06191 [hep-ph]`.

[20] A. V. Manohar, "Introduction to Effective Field Theories," `arXiv:1804.05863 [hep-ph]`.

[21] I. Brivio, S. Dawson, J. de Blas, G. Durieux, P. Savard, A. Denner, A. Freitas, C. Hays, B. Pecjak, and A. Vicini, "Electroweak input parameters," `arXiv:2111.12515 [hep-ph]`.

[22] A. Biekötter, B. D. Pecjak, D. J. Scott, and T. Smith, "Electroweak input schemes and universal corrections in SMEFT," *JHEP* **07** (2023) 115, `arXiv:2305.03763 [hep-ph]`.

[23] V. Dūdėnas and M. Löschner, "Vacuum expectation value renormalization in the Standard Model and beyond," *Phys. Rev. D* **103** no. 7, (2021) 076010, `arXiv:2010.15076 [hep-ph]`.

[24] D. R. Yennie, S. C. Frautschi, and H. Suura, "The infrared divergence phenomena and high-energy processes," *Annals Phys.* **13** (1961) 379–452.

[25] J. Kublbeck, M. Bohm, and A. Denner, "Feyn Arts: Computer Algebraic Generation of Feynman Graphs and Amplitudes," *Comput. Phys. Commun.* **60** (1990) 165–180.

[26] T. Hahn, "Generating Feynman diagrams and amplitudes with FeynArts 3," *Comput. Phys. Commun.* **140** (2001) 418–431, `arXiv:hep-ph/0012260`.

[27] V. Shtabovenko, R. Mertig, and F. Orellana, "New Developments in FeynCalc 9.0," *Comput. Phys. Commun.* **207** (2016) 432–444, `arXiv:1601.01167 [hep-ph]`.

[28] V. Shtabovenko, R. Mertig, and F. Orellana, "FeynCalc 9.3: New features and improvements," *Comput. Phys. Commun.* **256** (2020) 107478, `arXiv:2001.04407 [hep-ph]`.

[29] V. Shtabovenko, R. Mertig, and F. Orellana, "FeynCalc 10: Do multiloop integrals dream of computer codes?," *Comput. Phys. Commun.* **306** (2025) 109357, `arXiv:2312.14089 [hep-ph]`.

[30] A. Denner, "Techniques for calculation of electroweak radiative corrections at the one loop level and results for W physics at LEP-200," *Fortsch. Phys.* **41** (1993) 307–420, `arXiv:0709.1075 [hep-ph]`.

[31] L. Darmé *et al.*, "UFO 2.0: the 'Universal Feynman Output' format," *Eur. Phys. J. C* **83** no. 7, (2023) 631, `arXiv:2304.09883 [hep-ph]`.

[32] A. Dedes, J. Rosiek, M. Ryczkowski, K. Suxho, and L. Trifyllis, "SmeftFR v3 – Feynman rules generator for the Standard Model Effective Field Theory," *Comput. Phys. Commun.* **294** (2024) 108943, `arXiv:2302.01353 [hep-ph]`.

[33] S. Frixione, Z. Kunszt, and A. Signer, "Three jet cross-sections to next-to-leading order," *Nucl. Phys. B* **467** (1996) 399–442, `arXiv:hep-ph/9512328`.

[34] T. D. Lee and M. Nauenberg, "Degenerate Systems and Mass Singularities," *Phys. Rev.* **133** (1964) B1549–B1562.